JOC The Journal of Organic Chemistry

Article

pubs.acs.org/joc

Mechanistic Origins of Chemo- and Regioselectivity of Ru(II)-Catalyzed Reactions Involving *ortho*-Alkenylarylacetylene, Alkyne, and Methanol: The Crucial Role of a Chameleon-like Intermediate

Yanfeng Dang,[†] Shuanglin Qu,[†] Yuan Tao,[†] Chunyu Song,[†] and Zhi-Xiang Wang*[,†,‡]

[†]School of Chemistry and Chemical Engineering, University of the Chinese Academy of Sciences, Beijing 100049, China

[‡]Collaborative Innovation Center of Chemical Science and Engineering, Tianjin 300072, China

Supporting Information

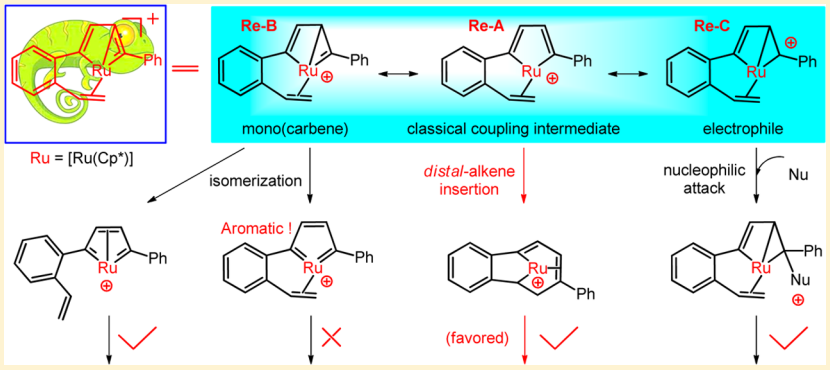

ABSTRACT: M06-DFT computations have been applied to understand four catalytic systems which involved $[Ru(Cp^*)(MeCN)_3]PF_6$ or $[Ru(Tp)(PPh_3)(MeCN)_2]PF_6$ as mediator and *ortho*-alkenylarylacetylene, terminal alkyne, and methanol as reactants. Potentially, the products of these systems could be dihydrobiphenylenes, 1,3-dienyl ether, and naphthalene. Remarkably, each system afforded product selectively. Our computed mechanisms successfully account for the chemo- and regioselectivities of these systems. Furthermore, the study demonstrates that the chameleon-like mono(carbene) intermediates formed via the intermolecular alkyne−alkyne oxidative coupling play a crucial role to complete the reactions. According to their geometric and electronic structures, three resonance structures were introduced to characterize their reactivity properties, which address the features of the classical alkyne−alkyne oxidative coupling intermediates, mono(carbene) species, and electrophilicity of the intermediates, respectively. The reactivity properties lead to three channels isomerizing the intermediates to three isomers. Surprisingly, the bis(carbene) isomers, which are similar to the bis(carbene) intermediates generally considered to be crucial in the neutral RuCp*Cl-catalyzed systems, are accessible but not reactive enough to continue the subsequent reaction steps partially due to aromaticity. The other two isomers continue subsequent reaction steps. These findings may help not only to understand the four specific catalytic reactions but also to advance the [2 + 2 + 2] synthetic methodology.

1. INTRODUCTION

Transition metal (TM)-catalyzed cycloaddition is an effective synthetic methodology to construct carbo- and heterocycles,[1] among which [2 + 2 + 2] cycloaddition produces hexacycles.[2] Since Reppe et al.'s seminal report of TM-catalyzed cyclotrimerization of alkynes to synthesize benzene derivatives,[3] various [2 + 2 + 2] cycloaddition reactions have been developed.[2−6] The substrates range alkynes, diynes, alkenes, imines, isocyanates, and isothiocyanates; the catalysts cover Co, Ru, Rh, Ir, Ni, Pd, Mn, Cr, Fe, Zr, Nb, and Ta-based complexes; and the products include benzenes, pyridines, pyridones, pyrones, and other six-membered cycles. Moreover, these reactions tolerate functional groups such as alcohols, amines, alkenes, ethers, esters, halogens, and nitriles.

Biphenylene and its derivatives are useful building units in chemical synthesis and in making functionalized organic materials.[7] Previously, the synthesis of biphenylenes mainly relied on ring-closure reactions, where the cyclobutadiene ring is formed either by dimerization of benzynes or by coupling reactions.[8] On the basis of the [2 + 2 + 2] cycloaddition methodology,[9] Saá, Esteruelas, and co-workers recently developed a novel route to synthesize dihydrobiphenylenes (eqs 1 and 2).[10] They reported that, under the catalytic influence of the $[Ru(Cp^*)(MeCN)_3]PF_6$ complex **Ru1**,[11] *ortho*-alkenylarylacetylene **1a** underwent [2 + 2 + 2] dimerization to afford **1b** (eq 1, system 1), but in the presence of terminal alkyne **2a**, **1a** preferentially reacted with **2a** via [2 + 2 + 2] cocyclization to give dihydrobiphenylene **2b** (eq 2, system 2). For the description convenience, we herein and hereafter use eq *X* and system *Y* (*X*, *Y* = 1−4) to

Received: June 23, 2014
Published: September 15, 2014

   dx.doi.org/10.1021/jo501399x | J. Org. Chem. 2014, 79, 9046−9064

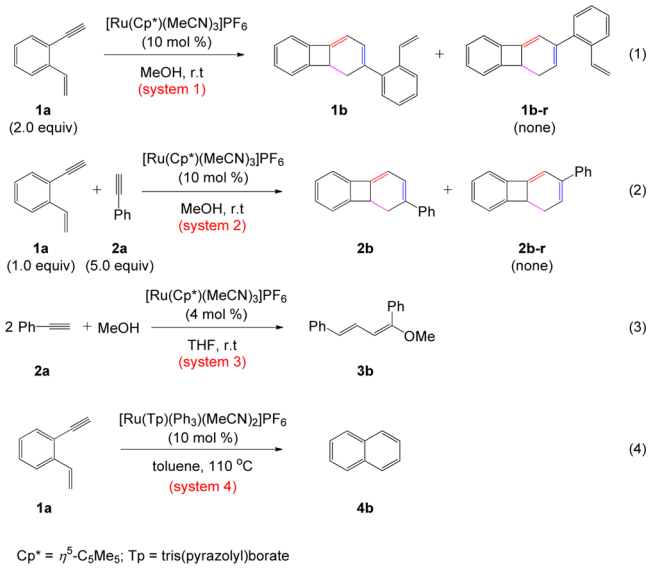

define a specific reaction channel occurring in a catalytic system. Equation 1 reaction could potentially occur in system 2 (i.e., dimerization versus cocyclization), but the two systems had perfect chemo- and regioselectivity to produce single product. In addition, the dimerization of **1a** and cocyclization of **1a** and **2a** could also give the regioisomers (**1b**−**r** and **2b**−**r**), respectively, but system 1 and 2 selectively gave **1b** and **2b**, respectively. The reactions were run in methanol solvent, but Dixneuf, Beller, and co-workers have found that the same **Ru1** complex promoted the reaction of terminal alkynes (e.g., **2a**) and methanol readily to give 1,3-dienyl ethers (e.g., **3b**) within several minutes at room temperature (eq 3, system 3).[12] Because **1a** in system 1 and 2 bears a terminal alkyne group and **2a** presented in system 2, it is surprising that such a facile reaction channel (neither eq 3 nor eq 3-like) did not take place in system 1 and 2. Intramolecular cyclization of **1a** to give naphthalene is thermodynamically favorable because of the aromatization effect. Liu and co-workers have realized this process by using $[Ru(Tp)(PPh_3)(MeCN)_2]PF_6$[13] complex **Ru2** (eq 4, system 4).[14] However, the aromatization of **1a** did not operate in systems 1 and 2, and conversely, eq 1 reaction did not take place in system 4. Intrigued by the chemo- and regioselectivity chemistries involved in these notable catalytic systems, as well as their catalytic mechanisms, we performed a comparative mechanistic study on the four reactions,[15] aiming at resolving these puzzles. In addition to successfully rationalizing the experimental products/observations, we characterized an unusual intermediate involved in system 2 or 3, which plays a crucial role to gear the reaction to the channel leading to the experimental product.

2. COMPUTATIONAL METHODS

All calculations were carried out with Gaussian 09[16] at the M06[17] level of density functional theory, which was developed by Truhlar group to target organometallic systems.[17−19] With the use of actual catalysts and substrates rather than truncated models, geometry optimizations and frequency calculations were performed at the M06/BS1 level in the gas phase, BS1 designating a mixed basis set of SDD[20] for Ru and 6-31G(d) for other atoms. Frequency analysis outcomes were examined to confirm the optimized structures as minima (no imaginary frequency) or transition states (only one imaginary frequency). With the use of the M06/BS1 optimized geometries, the energetic results were then improved by M06/BS2 single-point calculations with the solvent effects accounted by SMD[21] solvent model, using experimentally used solvents shown in eq 1−4. BS2 denotes a mixed basis set of SDD for Ru and 6-311++G(d,p) for other atoms. The M06/BS1 frequencies were used for thermal corrections to the M06/BS2 single-point energies, giving enthalpies and free energies at 298.15 K and 1 atm. Natural bond orbital (NBO) analyses were performed at the M06/BS2 level on selected structures. Free energies (in kcal/mol) obtained from the M06/BS2 single-point calculations were discussed, and enthalpies (in kcal/mol) were given for reference. *For clarity, the charge state of these monocationic reactions is not shown in some Figures and Schemes.* Additional computational results, total energies, and Cartesian coordinates of the optimized structures are given in Supporting Information.

3. RESULTS AND DISCUSSION

The study aims at gaining insight into the catalytic mechanisms of the four reactions (eq 1−4), on which we disclose the origins of the chemo- and regioselectivities involved in these catalytic systems. To reach the goal, we organize the sections as follow. In Section 3.1, we unveil the mechanisms of **Ru1**-mediated [2 + 2 + 2] cycloadditions, including the dimerization of **1a** (eq 1) and the cocyclization of **1a** and **2a** (eq 2). According to the mechanisms, we elucidate the chemoselectivity (dimerization vs cocyclization) and the regioselectivities (**1b** vs **1b**−**r** and **2b** vs **2b**−**r**), and reactivities of three other substrates, among which two were experimentally found ineffective to run the reactions (vide infra). Section 3.2 discloses the mechanism of eq 3, according to which we rationalize why eq 3 did not operate in system 1 and 2. On the basis of results in Sections 3.1 and 3.2, in Section 3.3, we introduce three resonance structures to characterize the reactivity properties of an important intermediate involved in eq 2 and 3, respectively, and to deeply understand the crucial role of the intermediate in the two reactions. Section 3.4 reports the aromatization mechanism of **1a** mediated by **Ru2** complex (eq 4), which enables us to understand why the thermodynamically favorable aromatization process did not operate in systems 1 and 2 and eq 1 did not occur in system 4.

3.1. Mechanisms, Regio- and Chemoselectivity for [2 + 2 + 2] Cycloadditions between *ortho*-Alkenylarylacetylenes and Alkynes. The **Ru1** complex $[Ru(Cp^*)(MeCN)_3]PF_6$ was applied to perform eq 1−3 reactions. The anionic PF_6^- component in **Ru1** is a spectator and plays no essential role in catalysis. Following the convention,[22] we only considered the cationic $[Ru(Cp^*)(MeCN)_3]^+$ (**1cat**) species in mechanistic computations. Experimentally, Saá, Esteruelas, and co-workers observed **2cat** by NMR spectrum at low temperature (Scheme 1).[10]

Scheme 1

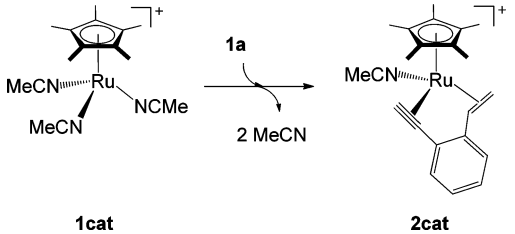

Supportively , the transformation of **1cat** + **1a** → **2cat** + 2*L(MeCN) was computed to be exergonic by 9.7 kcal/mol and the formations of other species are thermodynamically less favorable. Thus, we considered **1cat** to be a catalyst precursor and used **2cat** as the actual catalyst to compute the catalytic mechanisms.

dx.doi.org/10.1021/jo501399x | J. Org. Chem. 2014, 79, 9046−9064

Scheme 2. Possible Pathways for 2cat-Catalyzed [2 + 2 + 2] Cocyclization of 1a and 2a Leading to Product 2b

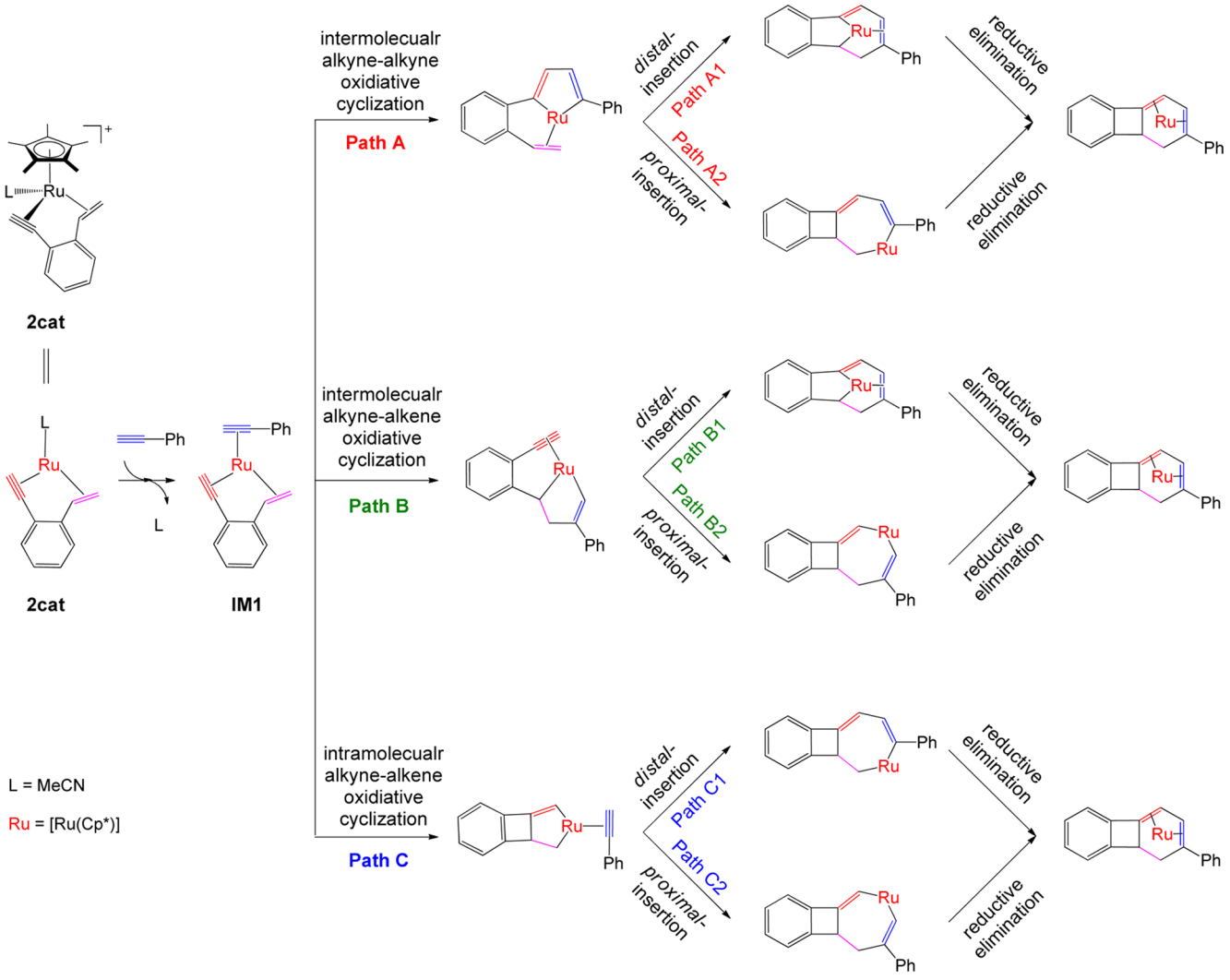

3.1.1. Mechanisms. Saá, Esteruelas, and co-workers have shown that the system 2 prefers the cocyclization of **1a** and **2a** to produce **2b** (eq 2), according to which, Scheme 2 sketches the possible pathways leading **1a** + **2a** to **2b**.[4−6,10,11,23] After replacing a labile MeCN ligand with **2a** in **2cat** to generate a Ru π-complex **IM1**, an oxidative coupling takes place. Depending on which two unsaturated groups couple first, three coupling modes are possible, namely, intermolecular alkyne−alkyne (CMA), intermolecular alkyne−alkene (CMB), and intramolecular alkyne−alkene (CMC) modes, respectively. Subsequent to the oxidative coupling, migratory insertion of the third unsaturated bond and reductive elimination proceed sequentially, finally affording the product **2b**. The migratory insertion can take place via either *distal*- or *proximal*-insertion. In mechanistic calculations, we took all the possible routes into consideration.

Figure 1 illustrates the catalytic mechanism for eq 2, and the optimized structures of key stationary points labeled in Figure 1 are displayed in Figure 2. The substitution of **2a** for a MeCN ligand in **2cat** resulting in an 18*e* Ru complex **IM1** is endergonic by 6.8 kcal/mol, explaining why **2cat** rather than **IM1** could be observed at low temperature. Among the three coupling modes in Scheme 2, the intermolecular alkyne−alkyene oxidative coupling (CMA) is superior to others; **TS1** is 3.5 and 28.5 kcal/mol lower than **TS6** for CMB and **TS7** for CMC couplings, respectively. Therefore, we first focused on the Path 1A initiated by CMA coupling. Relative to **2cat** + **2a**, the head-to-head oxidative coupling overcomes a barrier of 16.1 kcal/mol (**TS1**) and is exergonic by 1.6 kcal/mol. The resultant **IM2** complex features somewhat Fischer Ru-carbene character, as manifested by the length of the formal Ru═C^1 double bond (1.952 Å) and the NBO charge on C^1 (Q = 0.282*e*). We will deeply discuss the reactivity properties of **IM2** in Section 3.3. The oxidative couple promotes C^2−C^3 bond formation, as described by the gradually shortened C^2···C^3 distance, from 2.715 in **IM1** to 2.041 in **TS1** to 1.483 Å in **IM2**. Subsequently, **IM2** bifurcates, leading to Paths 1A1 and 1A2, respectively. **IM2** has a NBO charge population of C^1 = 0.282, C^4 = 0.020, C^5 = −0.167, and C^6 = −0.305*e*. The population suggests that the alkene *distal*-insertion of C^5═C^6 to Ru−C^1 forming Ru−C^5 and C^1−C^6 bonds would be preferred over the *proximal*-insertion of C^5═C^6 to Ru−C^4 forming Ru−C^6 and C^4−C^5 bonds. The preferred insertion only crosses a barrier of 0.1 kcal/mol (**TS2**), transforming **IM2** to **IM3** with releasing 24.0 kcal/mol of energy. We attempted to locate a TS for **IM2** isomerization via intramolecular *proximal*-insertion, but all optimizations repeatedly converged to **TS2** for *distal*-insertion. In **IM3**, the C^4−C^5 bond is not formed and a reductive elimination

dx.doi.org/10.1021/jo501399x | *J. Org. Chem.* 2014, 79, 9046−9064

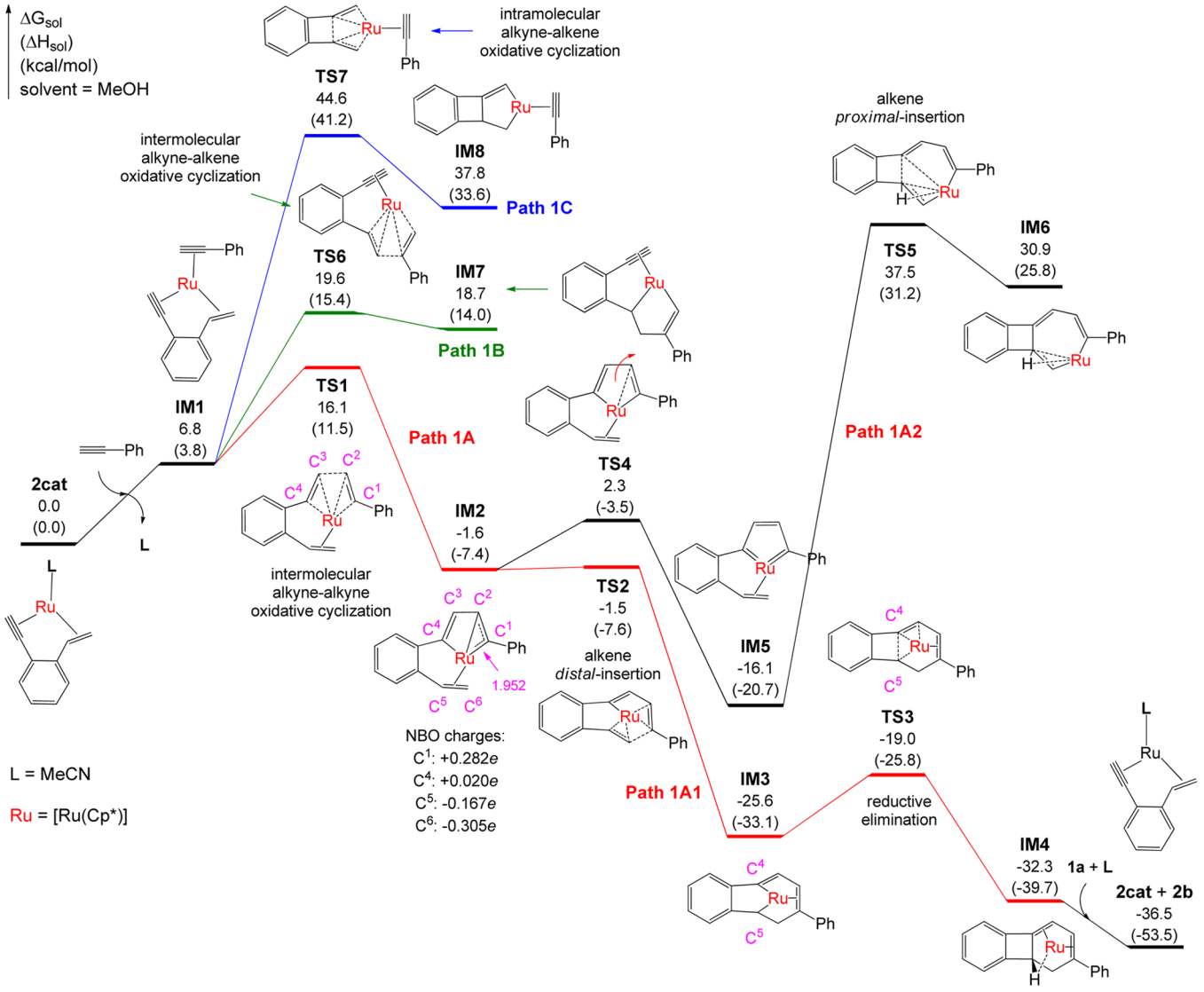

Figure 1. Free energy profiles for the **2cat**-catalyzed [2 + 2 + 2] cocyclization of **1a** and **2a** to give **2b**. Energies are relative to **2cat** + **2a** and are mass balanced.

process (**TS3**) promotes the bond formation, which is depicted by the gradually shortened $C^4\cdots C^5$ distance from 2.376 in **IM3** to 1.968 in **TS3** to 1.528 Å in **IM4**. The reductive elimination is feasible both kinetically and thermodynamically, crossing a barrier of 6.6 kcal/mol (**TS3**) and being exergonic by 6.7 kcal/mol. The reduction transfers **IM3** to **IM4** with the tricyclic product **2b** formed. **IM4** is a η^4-coordination complex with the $(RuCp^*)^+$ moiety coordinated to the two C=C double bonds of **2b**; thus, **2b** can be liberated without breaking a covalent bond, under the influence of solvent and substrate.[10] The generation of **2cat** + **2b** from **IM4** via association with **1a** + MeCN ligand is further exergonic by 4.2 kcal/mol.

The [2 + 2 + 2] cycloadditions mediated by neutral RuCp*Cl(COD) complex have been the subjects of experimental and computational studies,[2,4] showing that a bis(carbene) species is a crucial intermediate involved in these reactions. In Section 3.3, we will show that **IM2** is not a bis(carbene) species. By breaking $Ru-C^2$ bond via **TS4**, **IM2** can easily isomerize to **IM5** which features bis(carbene) characteristics. Interestingly, this process is very feasible with a barrier of only 3.9 kcal/mol (**TS4**) and an exergonicity of 14.5 kcal/mol, but still less favorable than the **IM2** → **TS2** → **IM3** isomerization in terms of both kinetics and thermodynamics. Subsequent to **IM5** formation, the *proximal*-insertion of $C^5{=}C^6$ π bond to $Ru-C^4$ via **TS5** needs to surmount a prohibitively high barrier (53.6 kcal/mol relative to **IM5**) mainly due to introducing a 4-ring in the TS, excluding this pathway. Note that **IM6** led by **TS5** can also result in product **2b** via reductive elimination. In **IM5**, the *distal*-insertion of $C^5{=}C^6$ into $Ru-C^1$ bond was also examined, but the relevant TS and intermediate could not be located. The loss of reactivity of **IM5** in the present cationic system is different from the [2 + 2 + 2] cycloaddition catalyzed by neutral RuCp*Cl(COD) catalyst, where an **IM5**-like bis(carbene) is a key intermediate to continue subsequent reaction steps (see Section 3.3 for more discussion).[2,4]

It is interesting that **IM2** prefers the *distal*-insertion of $C^5{=}C^6$ to $Ru-C^1$, while **IM5** favors the *proximal*-insertion of $C^5{=}C^6$ to $Ru-C^4$, which we attribute to the overall contribution of the following factors: (i) Because the $Ru-C^2$ bond in the ruffled ruthenapentacycle of **IM2** can break easily to release the strain, the *distal*-insertion can proceed by bilateral

dx.doi.org/10.1021/jo501399x | J. Org. Chem. 2014, 79, 9046−9064

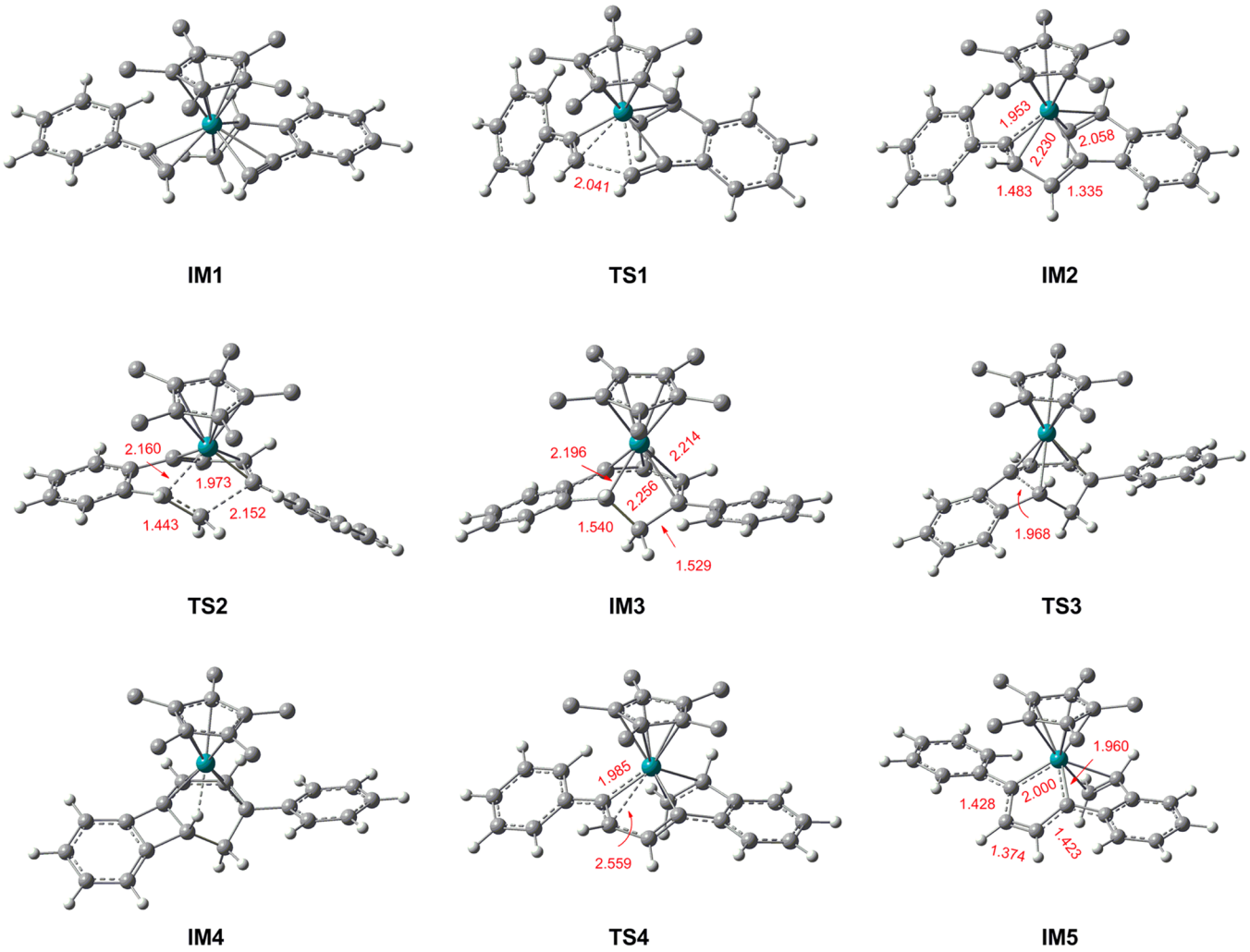

Figure 2. Key structures for **2cat**-catalyzed intermolecular [2 + 2 + 2] cycloaddition of **1a** and **2a**, with selected bond distances given in angstroms (Å). H atoms in the Cp* ligand are omitted for clarity.

migrations of $C^5{=}C^6$ and $Ru{-}C^1$. In contrast, the ruthenapentacycle in **IM5** is a rigid planar 5-ring; thus, the *distal*-insertion of $C^5{=}C^6$ to $Ru{-}C^1$ mainly relies on the unilateral migration of $C^5{=}C^6$ to $Ru{-}C^1$, but the migration is restrained by the chelated tail. (ii) As mentioned above, the electrostatic attraction in **IM2** favors *distal*-insertion to form $C^6{-}C^1$ bond over the *proximal*-insertion to $C^5{-}C^4$ bond, while such a preference in **IM5** is not significant because C^1 and C^4 are almost equally positively charged (C^1 = 0.119*e* and C^4 = 0.138*e*). (iii) The $C^5{\cdots}C^4$ and $C^6{\cdots}C^1$ distances in **IM5** are 2.630 and 3.025 Å, respectively, favoring *proximal*-insertion to form $C^5{-}C^4$ bond, while the two distances in **IM2** are 2.627 and 2.630 Å, respectively, without preferring to form one bond over another. Because all the TSs and intermediates in Path 1A1 are below **TS6** and **IM7** in Path 1B and **TS7** and **IM8** in Path 1C, we ruled out the two pathways led by the two (CMB and CMC) coupling modes.

3.1.2. Origins for Mechanistic Preference and Regioselectivity. Among the three coupling pathways (Path 1A–1C in Figure 1), Path 1A1 is most favorable. To understand the preference, Figure 3 contrasts the optimized structures of **TS1** and **TS6**. The coupling via **TS1** forms the $C^2{-}C^3$ bond where C^2 and C^3 only bear one H atom, respectively, while the coupling via **TS6** forms the $C^1{-}C^6$ bond where C^6 bears two H atoms and C^1 bears a large Ph group. Obviously, the steric hindrance between two (C^6-)H atoms and (C^1-)Ph in **TS6** is severer than that between two H atoms on the forming $C^2{-}C^3$ bond in **TS1**, as reflected by the significant $C^7{\cdots}H$ repulsion marked at 2.476 Å, which is shorter than the sum (2.9 Å) of van der Walls radii of C and H (R^{Cvdw} = 1.7 Å and R^{Hvdw} = 1.2 Å). As a consequence of steric hindrance, the benzene ring and $C^1{=}C^2$ π bond of **2a** part in **TS6** are distorted from the planar arrangement ($\angle C^2{-}C^1{-}C^7{-}C^8$ = 77.2° in **TS6**) for optimal π-conjugation, while the two parts in **TS1** tends to be in the same plane ($\angle C^2{-}C^1{-}C^7{-}C^8$ = 26.6°). Thus, **TS1** benefits from larger π conjugation effect than **TS6**. Although the H···H steric hindrances marked at 2.278 and 2.328 Å in **TS1** are absent in **TS6**, the favoring effect for **TS6** is not large enough to compensate the disfavoring effects for **TS6** caused by the steric hindrances due to the head-to-tail coupling. Overall, **TS1** is lower than **TS6** by 3.5 kcal/mol. **TS7** (see Supporting Information Figure S1 for its structure) involves a strained 4-ring, resulting in much higher **TS7** ($\Delta G^{\ddagger}$ = 44.6 kcal/mol) than **TS1** and **TS6**.

Of the two possible cocyclization products (**2b** and its regioisomer **2b–r**), the system 2 selectively produces **2b**. To unveil the origin of the regioselectivity, we computed the three possible pathways leading to **2b–r**, according to the coupling modes outlined in Scheme 2 (Supporting Information Scheme S1

dx.doi.org/10.1021/jo501399x | J. Org. Chem. 2014, 79, 9046–9064

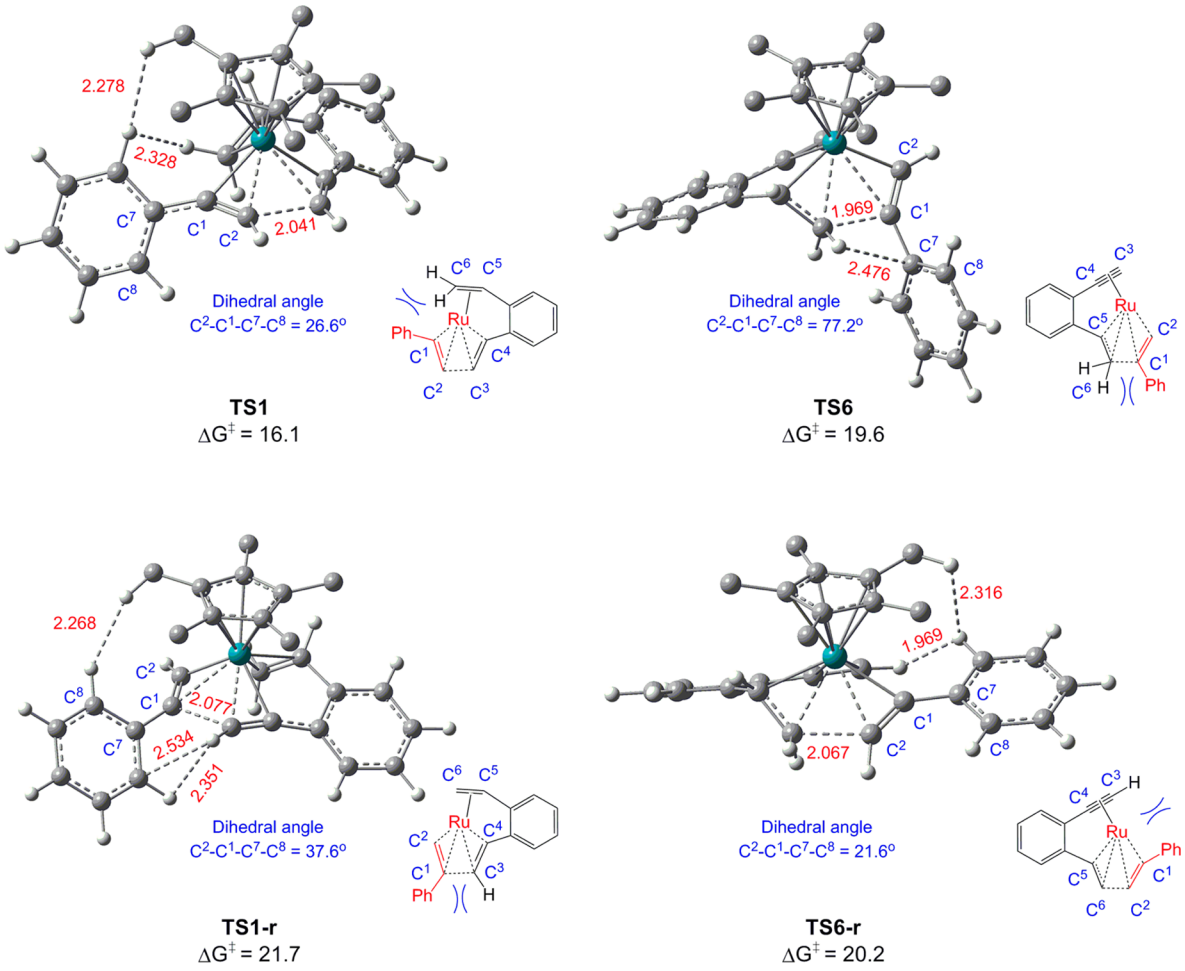

Figure 3. Optimized geometries and activation energies for the oxidative coupling TSs **TS1**/**TS6** (leading to **2b**) and **TS1-r**/**TS6-r** (leading to **2b**−**r**), with selected bond distances given in angstroms (Å). Trivial H atoms in Cp* ligand are omitted for clarity.

and S2). Different from the case leading to **2b** where CMA coupling mode is preferred, **TS6-r** for the CMB coupling mode was found to be the lowest among the three TSs to give **2b**−**r** (**TS1-r**, **TS6-r**, and **TS7-r**, which correspond to **TS1**, **TS6**, and **TS7**, respectively), with a relative energy of 20.2 kcal/mol, being 4.1 kcal/mol higher than **TS1** (Figure 3). The energetic difference accounts for the experimental regioselectivity of **2b** over **2b**−**r**.[10,24] In the following, we compare the structures of **TS1** and **TS6-r** to understand the causes for the regioselectivity.

Both **TS1** and **TS6-r** adopt the head-to-head coupling via intermolecular alkyne−alkyne and alkyne−alkene modes, respectively. Because the small size of H atom, the difference of steric effect between one (C^2)-H and one (C^3)-H in **TS1** and that between two (C^6)-H atoms and one (C^2)-H in **TS6-r** is unlikely to be a cause for the higher **TS6-r** than **TS1**. In addition, because the dihedral $\angle C^2{-}C^1{-}C^7{-}C^8$ in **TS1** (26.6°) is close to that (21.6°) in **TS6-r**, the π-conjugation between the benzene ring and $C^1{=}C^2$ π bond should not differ much in the two TSs. However, the shorter H···H distances in **TS6-r** (2.316 and 1.969 Å) than in **TS1** (2.278 and 2.328 Å) signify that **TS6-r** suffers steric hindrance between **2a** part and chelated **1a** part more severely than **TS1**, which could be a major factor for higher **TS6-r** than **TS1**.

As **TS1** is lower than **TS6** by 3.5 kcal/mol, conversely, **TS1-r** is higher than **TS6-r** by 1.5 kcal/mol. A major contributor for this could be the steric hindrance between (C^3)-H and (C^1)-Ph group in **TS1-r**, as indicated by the significant H···H and C···H repulsions marked at 2.351 and 2.534 Å. Comparisons of the steric hindrances in the four TSs (Figure 3) classify them into two patterns: **TS1** and **TS6-r** share the head-to-head coupling pattern featuring the sreric hindrances between Ph group of coupling **2a** and the methyl group of Cp* and H atom(s) of chelated **1a**. **TS6** and **TS1-r** shares the head-to-tail coupling pattern featuring the steric hindrances between the Ph group of the coupling **2a** and the H atom of chelated **1a**. Among the two patterns, the head-to-head coupling pattern (**TS1** and **TS6-r**) is energetically more favorable than the head-to-tail coupling pattern (**TS6** and **TS1-r**).[11] Similar to **TS7**, **TS7-r** for CMC coupling mode also involves a strained 4-ring, resulting much higher energy barrier ($\Delta G^{\ddagger}$ = 44.8 kcal/mol, Supporting Information Figure S1).

3.1.3. Chemoselectivity: Dimerization versus Cocyclization. We have shown that system 2 preferentially undergoes cocyclization to produce **2b** rather than **2b**−**r**. Experimentally, it has been found that in the absence of **2a** the same catalyst promoted **1a** to undergo [2 + 2 + 2] dimerization to produce **1b** (eq 1). To understand why eq 1 did not take place in system 2, we computed the pathway for **2cat**-catalyzed [2 + 2 + 2] dimerization of **1a** (see Figure 4 and Supporting Information Figure S2). Expectedly, the dimerization pathway of **1a** in blue resembles the one in red for cocyclization of **1a** and **2a**. However, all the stationary points in the blue pathway are

dx.doi.org/10.1021/jo501399x | J. Org. Chem. 2014, 79, 9046−9064

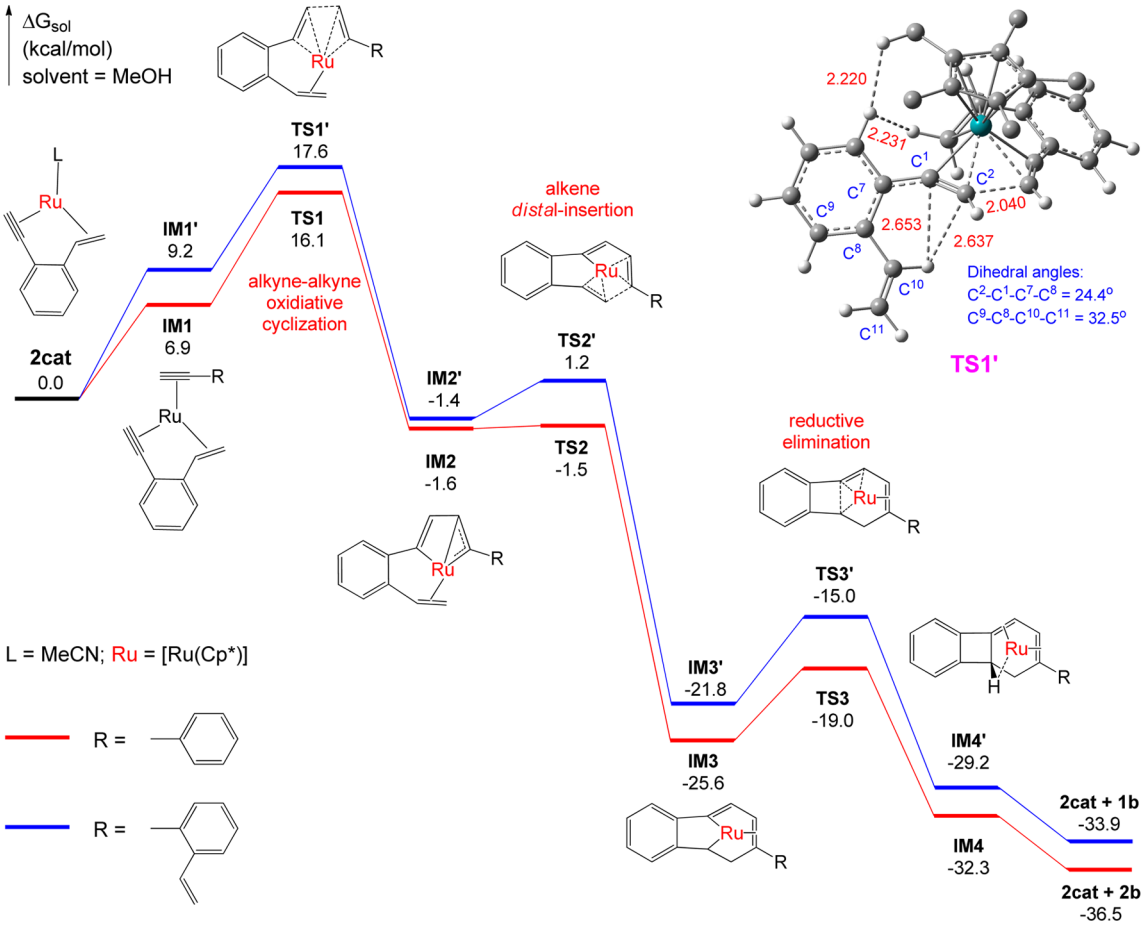

Figure 4. Free energy profiles for **2cat**-catalyzed [2 + 2 + 2] dimerization of **1a** (blue) and [2 + 2 + 2] cocyclization of **1a** with **2a** (red). Energies are relative to **2cat** and are mass balanced.

above their counterparts in the red one. For the rate-determining intermolecular alkyne−alkyne oxidative coupling step, **TS1′** is 1.5 kcal/mol higher than **TS1**, which agrees qualitatively with the experimental observation that the dimerization of **1a** (eq 1) was suppressed in system 2. On the other hand, the ratio (**1a**:**2a** = 1:5, experimental condition) of substrates in system 2 favors the cocyclization of **1a** and **2a**. This could be the reason the optimal catalytic condition needed to use excess **2a** to suppress eq 1 in system 2, because the energetic difference (1.5 kcal/mol) between **TS1** and **TS1′** is not large.

The optimized structure of **TS1′** is displayed in Figure 4. The difference of **TS1′** from **TS1** is the substitution of the (C^8)-H atom for a −CH═CH_2 group in **TS1**. The substitution causes steric hindrances between (C^{10})-H and C^1═C^2 bonds, as indicated by the C^1···H (2.653 Å) and C^2···H (2.637 Å) distances shorter than the 2.9 Å of R^{Cvdw} + R^{Hvdw}. The steric hindrance prevents minimizing the steric hindrance between the Ph group of coupling **1a** and the Cp* methyl group/(═C−)H atom of the chelated **1a**, as reflected by the H···H distances (2.220 and 2.231 Å) in **TS1′** shorter than those (2.278 and 2.328 Å) in **TS1**. The steric hindrance also distorts the ∠C^9−C^8−C^{10}−C^{11} dihedral angle (16.2°) in free **1a** to 32.5° in **TS1′**. The distortion results in strain and weakens π-conjugation, thus destabilizing **TS1′**. The same effect applies for the higher **IM1′** than **IM1** (9.2 vs 6.9 kcal/mol).

3.1.4. Reactivity. Experimentally, it has been reported that the (*Z*)-**3a** substrate was able to perform [2 + 2 + 2] dimerization to afford dihydrobiphenylene **5b** (eq 5), that of (*E*)-**3a** was not effective (eq 6), and that of the internal alkyne **5a** delivered no product (eq 7).[10] To account for the conformation influence

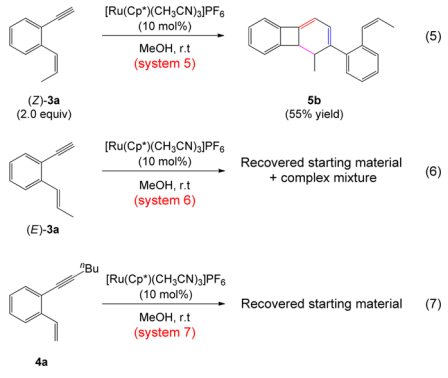

[i.e., (*Z*) vs (*E*)] on the reactivity, we based the mechanistic understanding on eqs 1 and 2 to optimize the two rate-determining TSs (**TS1-*Z*-3a** and **TS1-*E*-3a**) for dimerizations of (*Z*)-**3a** and (*E*)-**3a**, respectively. The energetic and geometric results are given in Figure 5 (see Supporting Information Figure S4 for more details). The difference between **TS1-*Z*-3a** and **TS1′** is the replacement of (C^{11})-H in **TS1′** with a methyl group. Because the methyl group in both coupling and chelated (*Z*)-**3a** in **TS1-*Z*-3a** is away from the active site, the methyl substitution only alters the dimerization barrier slightly to 16.8 from 17.6 kcal/mol of **TS1′**, indicating the comparable reactivities

dx.doi.org/10.1021/jo501399x | J. Org. Chem. 2014, 79, 9046−9064

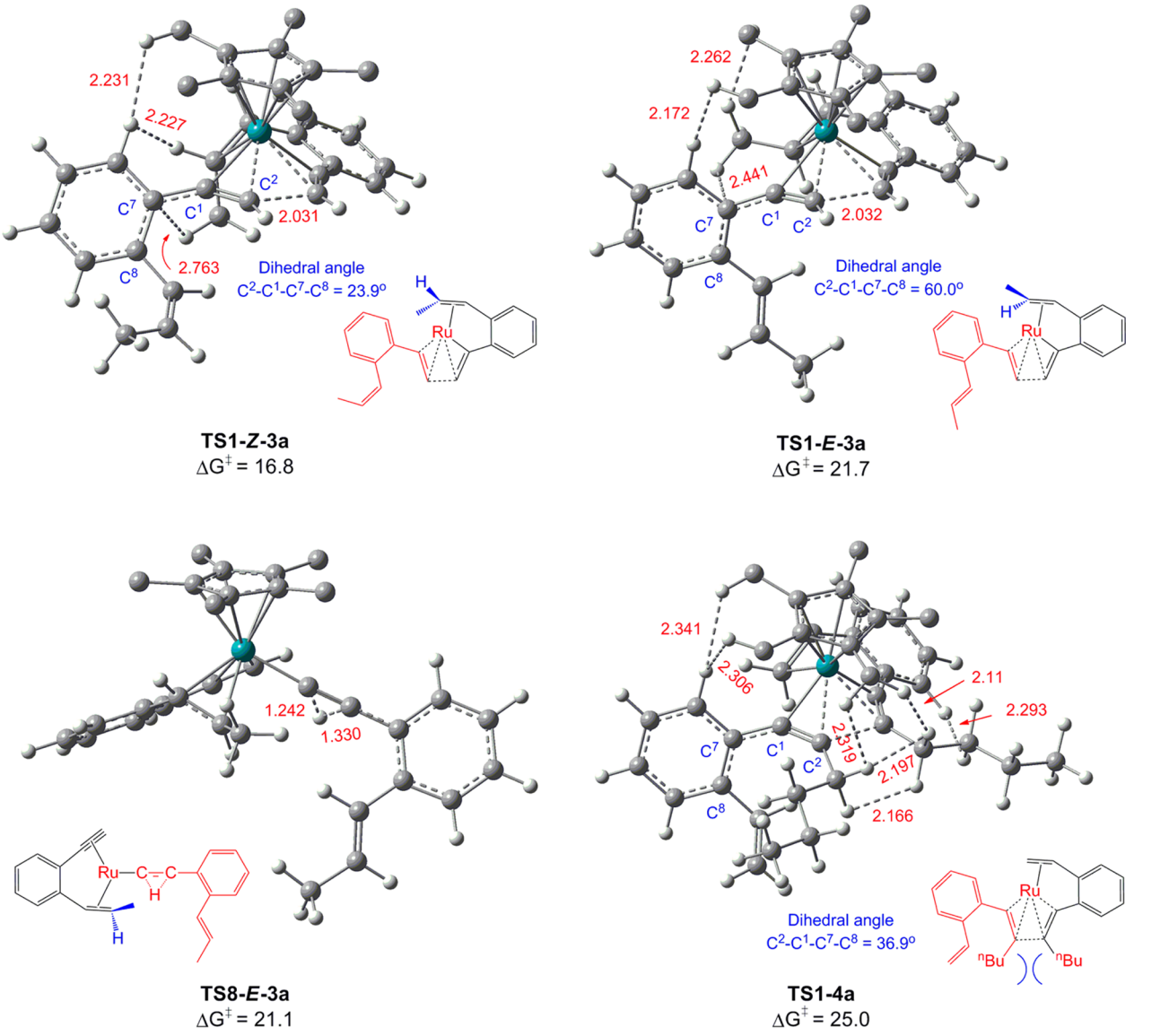

Figure 5. Optimized geometries and activation energies for the oxidative coupling TSs (**TS1-*Z*-3a**, **TS1-*E*-3a**, and **TS1-4a**) and the H-transfer TS (**TS8-*E*-3a**), with selected bond distances given in angstroms (Å). Trivial H atoms in Cp* ligand are omitted for clarity.

of (*Z*)-**3a** and **1a**. For the dimerization of (*E*)-**3a**, the methyl group of chelated (*E*)-**3a** in **TS1-*E*-3a** is *cis* to the Cp* ligand. Thus, there are enhanced steric hindrances between the coupling (*E*)-**3a** and the chelated (*E*)-**3a**/Cp* ligand, as indicated by the H···H repulsion marked at 2.172 Å and C···H repulsion marked at 2.441 Å. The hindrances also distort the dihedral angle of $C^2-C^1-C^7-C^8$ to 60.0° in the coupling of (*E*)-**3a**, weakening the π-conjugation between $C^1{=}C^2$ π bond and benzene ring. The overall contributions of these disfavoring effects account for why **TS1-*E*-3a** is 4.9 kcal/mol higher than **TS1-*Z*-3a**, thus (*E*)-**3a** is less reactive than (*Z*)-**3a** to undergo [2 + 2 + 2] dimerization.

To understand the observed mixture of products of system 6, we examined the aromatization reaction catalyzed by **2cat**. The formation of Ru-vinylidene complex is the rate-determining step in aromatization (see Section 3.4 for more details). **TS8-*E*-3a** is the TS to form Ru—vinylidene complex (Supporting Information Figure S3). Because **TS8-*E*-3a** and **TS1-*E*-3a** are not too high and the energetic difference between the two TSs is small (0.6 kcal/mol), the [2 + 2 + 2] dimerization and aromatization could proceed competitively, explaining the observation of mixed products in system 6. We speculate the mixture could contain aromatization product (**4b**-like compound). For (*Z*)-**3a** to undergo aromatization, the TS to form the Ru—vinylidene complex is 4.9 kcal/mol higher than **TS1-*Z*-3a**; thus, aromatization was suppressed in system 5 (Supporting Information Figure S4). The structure of **TS1—4a** in Figure 5 accounts for the loss of reactivity of **4a**, because of the large steric hindrance between the bulky ^{n}Bu groups. The dimerization barrier of **4a** ($\Delta G^{\ddagger}$ = 25.0 kcal/mol, **TS1—4a**) are substantially higher than the 17.6 kcal/mol (**TS1′**) and 16.8 kcal/mol of **TS1-*Z*-3a**, indicating that **4a** is indeed less reactive than **1a** and (*Z*)-**3a** in [2 + 2 + 2] dimerization.

3.2. [2 + 2 + 2] Cycloaddition versus Formation of 1,3-Dienyl Ether.

3.2.1. Mechanism for Equation 3. Dixneuf, Beller, and coworkers reported that the same complex **Ru1** as used in systems 1 and 2 could promote the reactions of terminal alkynes with alcohols easily to produce 1,3-dienyl ethers (eq 3).[12] These reactions could be completed in a few minutes at room

dx.doi.org/10.1021/jo501399x | J. Org. Chem. 2014, 79, 9046−9064

Scheme 3. Proposed Mechanism for the Formation of 1,3-Dienyl Ether

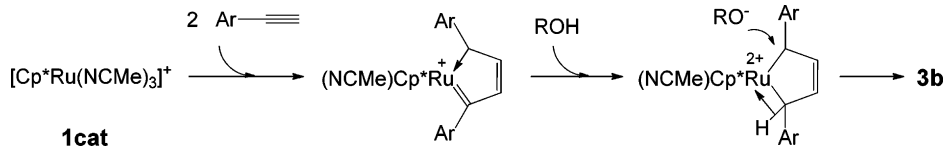

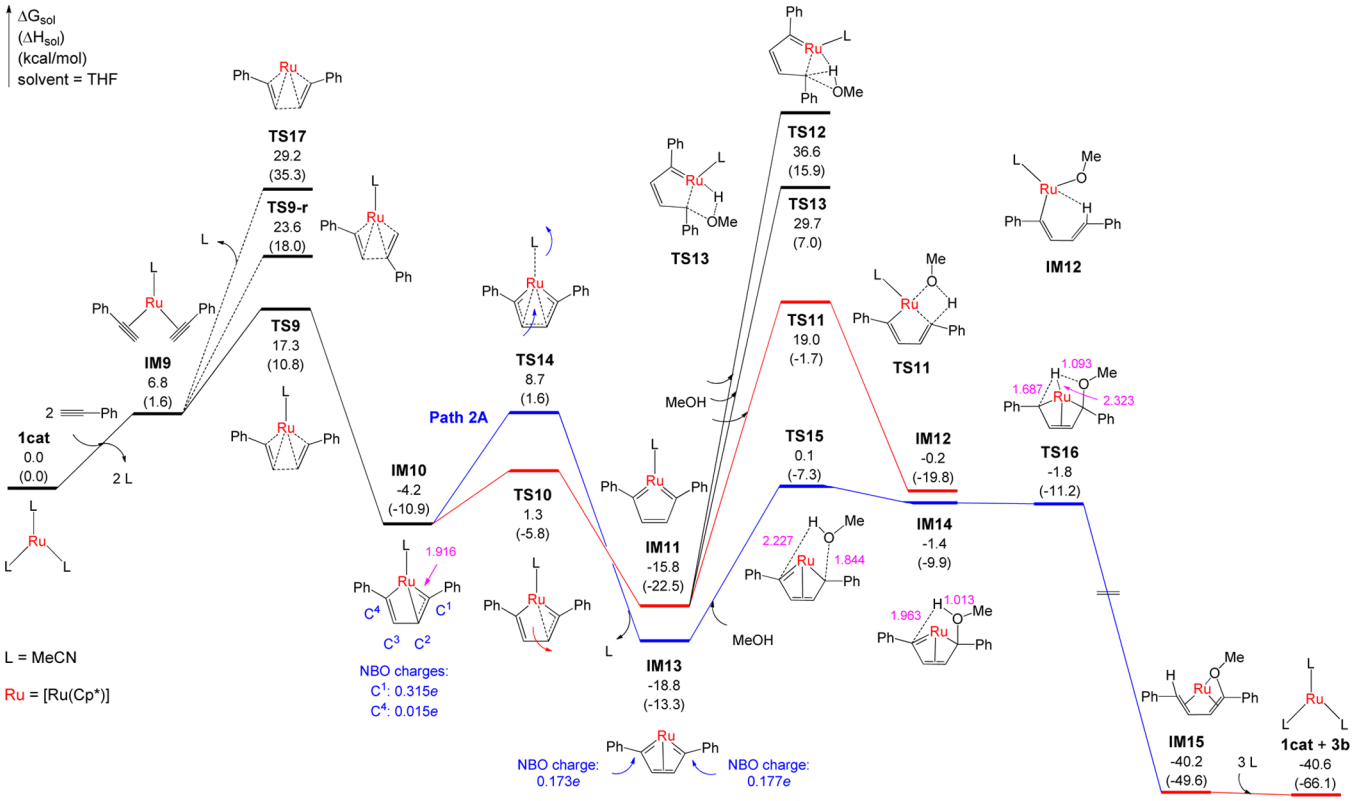

Figure 6. Free energy profiles for **1cat**-catalyzed synthesis of 1,3-dienyl ether **3b** from **2a** and methanol. Energies are relative to **1cat** and are mass balanced.

temperature with high yields (up to 96%). Considering the facts that systems 1 and 2 contained the terminal alkyne substrates (**1a** and **2a**) and used the same **Ru1** as mediator and methanol as solvent, it is surprising that the facile eq 3 or eq 3-like reaction did not operate in systems 1 and 2. To solve the puzzle, we first disclose the mechanism for eq 3, according to which, we then understand why eq 3 did not take place in systems 1 and 2.

Experimentalists have postulated a mechanism for the reaction (Scheme 3), which involves a bis(carbene) intermediate, $[RuCp^*(NCMe)(2,5\text{-}Ar_2C_4H_2)]^+$, formed from the head-to-head coupling of two terminal alkynes.[12] The intermediate was proposed to feature mixed Fischer- and Schrock-type carbene characteristics. The mechanism was previously applied for understanding reactions of terminal alkynes (ArC≡CH) with carboxylic acids RCO_2H to give dienylesters ArCH=CH−CH=CH−OOCR, under the catalytic influence of neutral RuCp*Cl(COD) complex.[25] Recently, Yamamoto has demonstrated the mechanism computationally.[25c] However, the same RuCp*Cl(COD) complex is not able to promote eq 3 reaction, implying that the mechanism for neutral catalytic system may not be applicable to the present cationic system. Figures 6 and 7 detail our mechanism for the **1cat**-catalyzed reaction of **2a** with methanol. The optimized structures of the key stationary points are displayed in Figure 8.

Initially, two **2a** molecules replace two liable MeCN ligands in **1cat** to give an 18*e* Ru π-complex (**IM9**) at an energetic cost of 6.8 kcal/mol (Figure 6). Subsequently, **IM9** undergoes head-to-head alkyne oxidative coupling via **TS9**, leading to **IM10**. Relative to **1cat**, the coupling crosses a barrier of 17.3 kcal/mol and is exergonic by 4.2 kcal/mol. **IM10** is similar to **IM2** and features Fischer mono(carbene) characteristics with a Ru=C bond length of 1.916 Å and a positively charged C^1 center (Q = 0.315*e*). From **IM9** to **TS9** to **IM10**, the forming C···C bond distance is gradually shortened from 2.666 to 1.984 to 1.478 Å, confirming the coupling process. We also examined two alternative coupling modes, including head-to-tail coupling, described by **TS9-r** and the coupling with a MeCN ligand dissociated from **IM9**, depicted by **TS27**; however, the two alternatives are much less favorable and we thus stopped pursuing the alternatives. Subsequently, the resulting **IM10** isomerizes to **IM11** [a bis(carbene) which will be further discussed in Section 3.3] easily with an energy barrier of 5.5 kcal/mol and an exergonicity of 11.6 kcal/mol. In the formation of dienylesters from terminal alkynes ArC≡CH with carboxylic acids RCO_2H, catalyzed by neutral RuCp*Cl(COD) complex, a proton transfer (H-transfer) from carboxylic group to Ru−C^α bond was proposed to be a key step,[25] based on which a H-transfer step from methanol to bis(carbene)-RuCp*$(NCMe)^+$

dx.doi.org/10.1021/jo501399x | J. Org. Chem. 2014, 79, 9046−9064

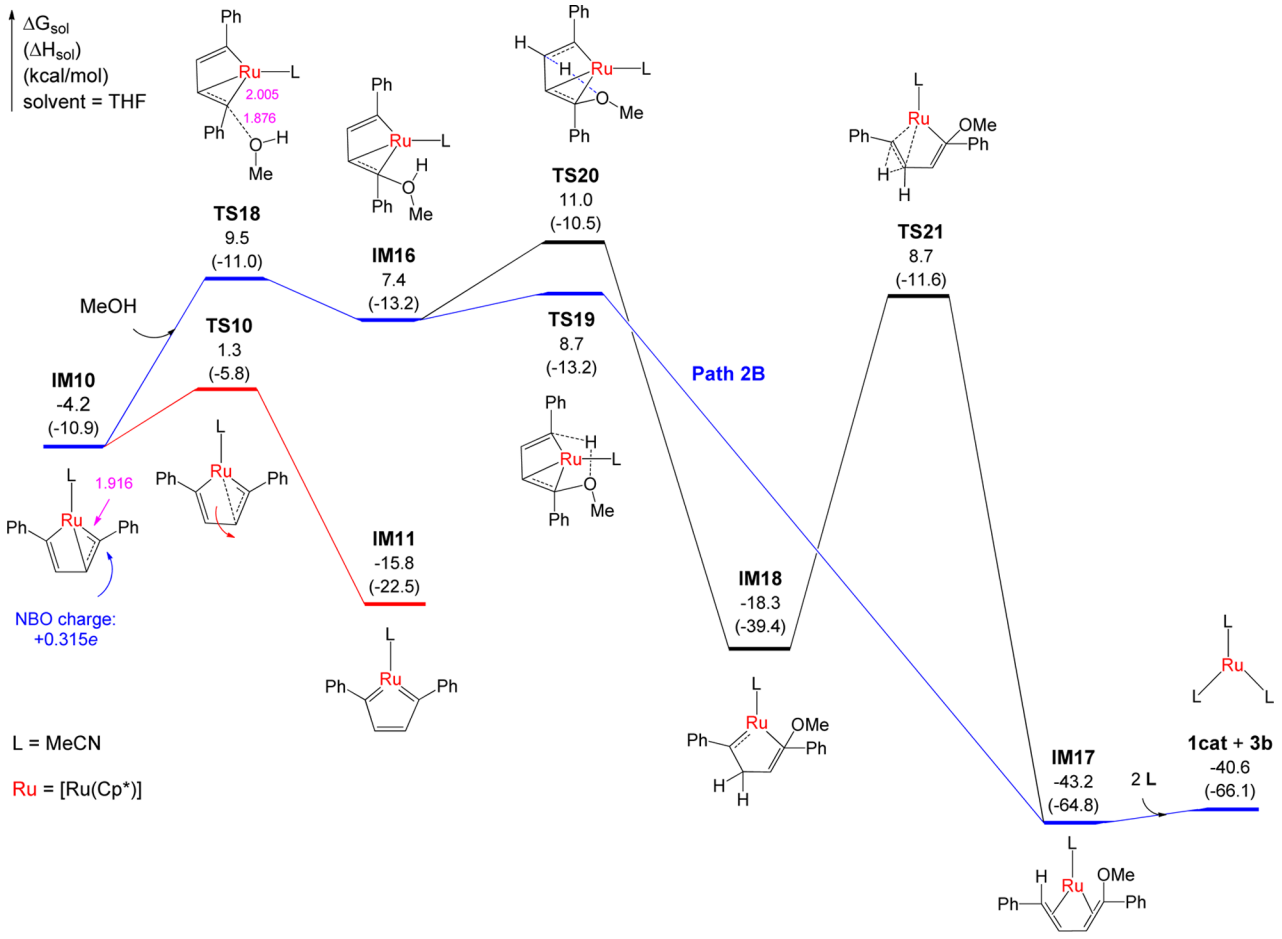

Figure 7. Free energy profiles for **1cat**-catalyzed synthesis of 1,3-dienyl ether **3b** from **2a** and methanol. Energies are relative to **1cat** and are mass balanced.

was suggested to account for eq 3. Accordingly, we examined the energy barrier for transferring methanol hydroxyl H to the C^1 (C^α) of **IM11**, leading to **IM12**, as illustrated by **TS11**. The large H-transfer energy barrier (34.8 kcal/mol) appears too high for eq 3 to take place quickly at room temperature. We also examined other H-transfer mechanisms depicted by **TS12** and **TS13**. The alternatives need to surmount even higher energy barriers [52.4 (**TS12**) and 45.5 kcal/mol (**TS13**)]. Therefore, we speculated that the H-transfer mechanism for the reactions of ArC≡CH with carboxylic acids in the neutral RuCp*Cl(COD) catalytic system does not apply to eq 3 in this cationic catalytic system, encouraging us to find new mechanisms via methanol nucleophilic attack.

First, we examined if the MeCN ligand of **IM10** can be dissociated to generate an intermediate susceptible to methanol attack, as illustrated by the **IM10** → **TS14** → **IM13** pathway (Path 2A in blue, Figure 6). Although the dissociation barrier (**TS14**) is 7.4 kcal/mol higher than that for **TS10**, it is significantly lower than that for **TS11**, **TS12**, and **TS13**. Furthermore, the resulting bis(carbene) **IM13** [see Section 3.3 for more discussion about the bis(carbene) feature] is lower than **IM11**. The energetic result implies a potentially feasible pathway to lead **IM13** + methanol to product **3b**. On the other hand, **IM13** has NBO charges of +0.177*e* and +0.173*e* on the two carbene atoms, which is desirable for methanol nucleophilic attack at the carbon atoms. Our computations showed the methanol nucleophilic attack could take place via crossing a barrier of 18.9 kcal/mol (**TS15** relative to **IM13**), resulting in **IM14**. The hydroxyl O−H bond in **IM14** does not cleave, but with the aid of Ru center, the hydroxyl H atom can migrate to another carbene carbon freely. **TS16** could be located in terms of electronic energy, but disappears after corrected by the solvent effects and thermal corrections. The methanol nucleophilic attack gives **IM15** with (1*Z*,3*E*) *s-cis*-**3b** moiety coordinated to $(RuCp^*)^+$ moiety. The exchange of three MeCN ligands with **3b** in **IM15** liberates the (1*Z*,3*E*) *s-cis*-**3b** and regenerates **1cat**. Then the (1*Z*,3*E*) *s-cis*-**3b** rotates around the C−C single bond by crossing a barrier of 4.8 kcal/mol, giving 3.9 kcal/mol more stable (1*Z*,3*E*) *s-trans*-**3b** (Supporting Information Figure S5). Noting that a (1*E*,3*E*) *s-trans*-**3b** configuration was reported experimentally (see eq 3), we tried to locate a pathway probably leading to (1*E*,3*E*) *s-trans*-**3b**, but were unsuccessful (see Supporting Information Figure S6 for more analyses). Furthermore, (1*E*,3*E*) *s-trans*-**3b** is 1.9 kcal/mol less stable than (1*Z*,3*E*) *s-trans*-**3b**. We call further experimental verification of the configuration of **3b**. The whole reaction of 2***2a** + MeOH → *s-trans*-**3b** is exergonic by 40.6 kcal/mol.

Second, we examined the direct methanol nucleophilic attack to **IM10** (without dissociating its MeCN ligand (Path 2B in blue, Figure 7), because **IM10** bears a positive charge of +0.315*e* on C^1. The methanol attack at the electrophilic C^1 atom also crosses a low barrier of 13.7 kcal/mol (**TS18**). The hydroxyl O−H bond in **IM16** led by **TS18** does not cleave and can be broken via two pathways. **TS19** describes the O−H

dx.doi.org/10.1021/jo501399x | J. Org. Chem. 2014, 79, 9046−9064

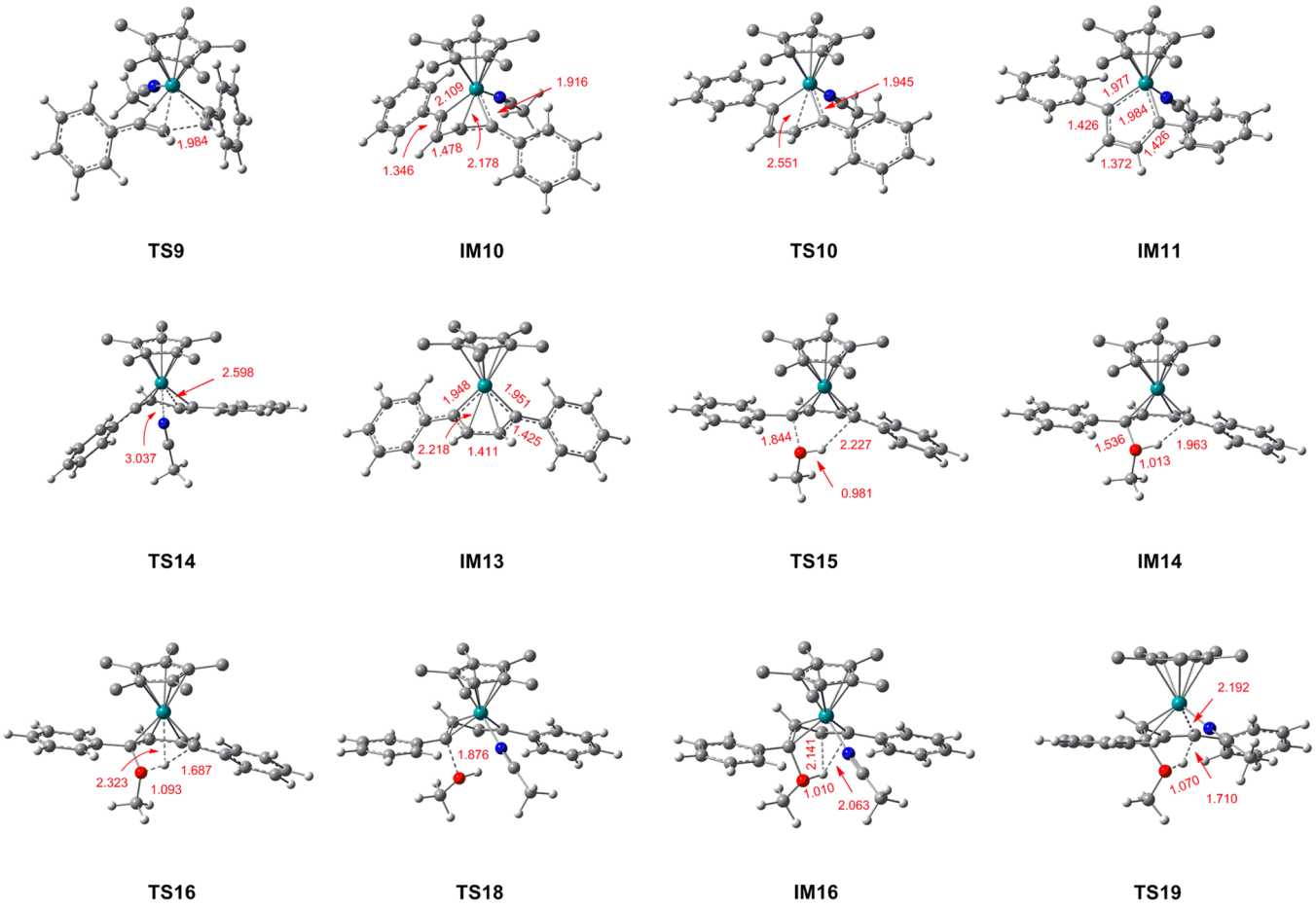

Figure 8. Key structures for **1cat**-catalyzed synthesis of **3b** from **2a** and methanol, with selected bond distances given in angstroms (Å). H atoms in the Cp* ligand are omitted for clarity.

bond breaking via H-transfer to C^4 with a barrier of 1.3 kcal/mol, leading to the more stable **IM17** with *s-cis*-**3b** coordinated to $(RuCp^*L)^+$ moiety. The alternative migrates hydroxyl H to C^3 via a 5-ring TS (**TS20**), leading to **IM18** which then undergoes 1,2-H-transfer to reach **IM17**. Expectedly, the former via **TS19** is more favorable than the latter via **TS20** by 2.3 kcal/mol, because of the less strained 6-ring **TS19** than the 5-ring **TS20**.

We now compare the favorability of Path 2A and Path 2B which start from **IM13** and **IM10**, respectively. For Path 2A, because **TS14** is 7.4 kcal/mol higher than **TS10**, **IM10** would isomerize to **IM11** through **TS10** preferentially. Subsequently, the metastable intermediate **IM11** transforms to **IM13** via the route (→**TS10** → **IM10** → **TS14** → **IM13**). An indirect support for the roundabout mechanism is that complexes similar to **IM11** in the neutral RuCp*Cl-catalyzed reactions have been crystallized.[26] This could be the reason **IM11** was considered to be the intermediate for methanol H-transfer giving **3b**. Along the roundabout pathway, the effective barrier for Path 2A should be estimated with respect to **IM11**, which gives a 24.5 kcal/mol of effective barrier. Similarly, Path 2B is estimated to have an effective barrier of 25.3 kcal/mol (the energetic difference between **IM11** and **TS18**). The small difference of the effective barriers (0.8 kcal/mol) of the two pathways indicates the both pathways are possible and they are competitive. We recall attention to that the mechanism via directly transferring methanol hydroxyl H to the C^{α} of **IM11**, which is similar to the reaction of terminal alkynes with carboxylic acids catalyzed by the RuCp*Cl(COD) complex, is not feasible in this cationic catalytic system. The mechanistic difference between the two systems can be attributed to the fact that proton in carboxylic acid is more acidic than that in methanol.

3.2.2. Origins for Not Producing 1,3-Dienyl Ether in Systems 1 and 2. After understanding the mechanism for eq 3, we now find why eq 3 did not occur in systems 1 and 2. Because eq 1 is less favorable than eq 2 (see Section 3.1), we only need to consider why eq 3 did not occur in system 2. Figure 9 compares the energetics of eqs 2 and 3. From **1cat** to **2cat**, replacement of the two MeCN ligands with the chelating ligand (**1a**) drives the system down by 9.7 kcal/mol. In contrast, the replacement of two MeCN ligands with two **2a** molecules for eq 3 raises the system by 3.9 kcal/mol. Thus, the initiation step of eq 2 is thermodynamically more favorable than that of eq 3. Furthermore, **TS1** for the intermolecular alkyne−alkyne oxidative coupling to enable eq 2 ([2 + 2 + 2] cycloaddition to give **2b**) is 8.0 kcal/mol lower than **TS9** for the oxidative coupling to enable eq 3 to produce **3b**, kinetically disfavoring eq 3. In terms of enthalpy, **IM1** and **TS1** in eq 2 pathway are even slightly higher than their counterparts (**IM9** and **TS9**) in eq 3 pathway. Thus, it is the entropy contribution that reverses the free energy orders; the chelation of **1a** ligand suffers less entropy penalty than the coordination of two separate **2a** alkyne ligands. It appears that the less entropy of **1a** than two separate **2a** plays a key role for the chemoselectivity of **2b** over **3b** in system 2.

dx.doi.org/10.1021/jo501399x | J. Org. Chem. 2014, 79, 9046−9064

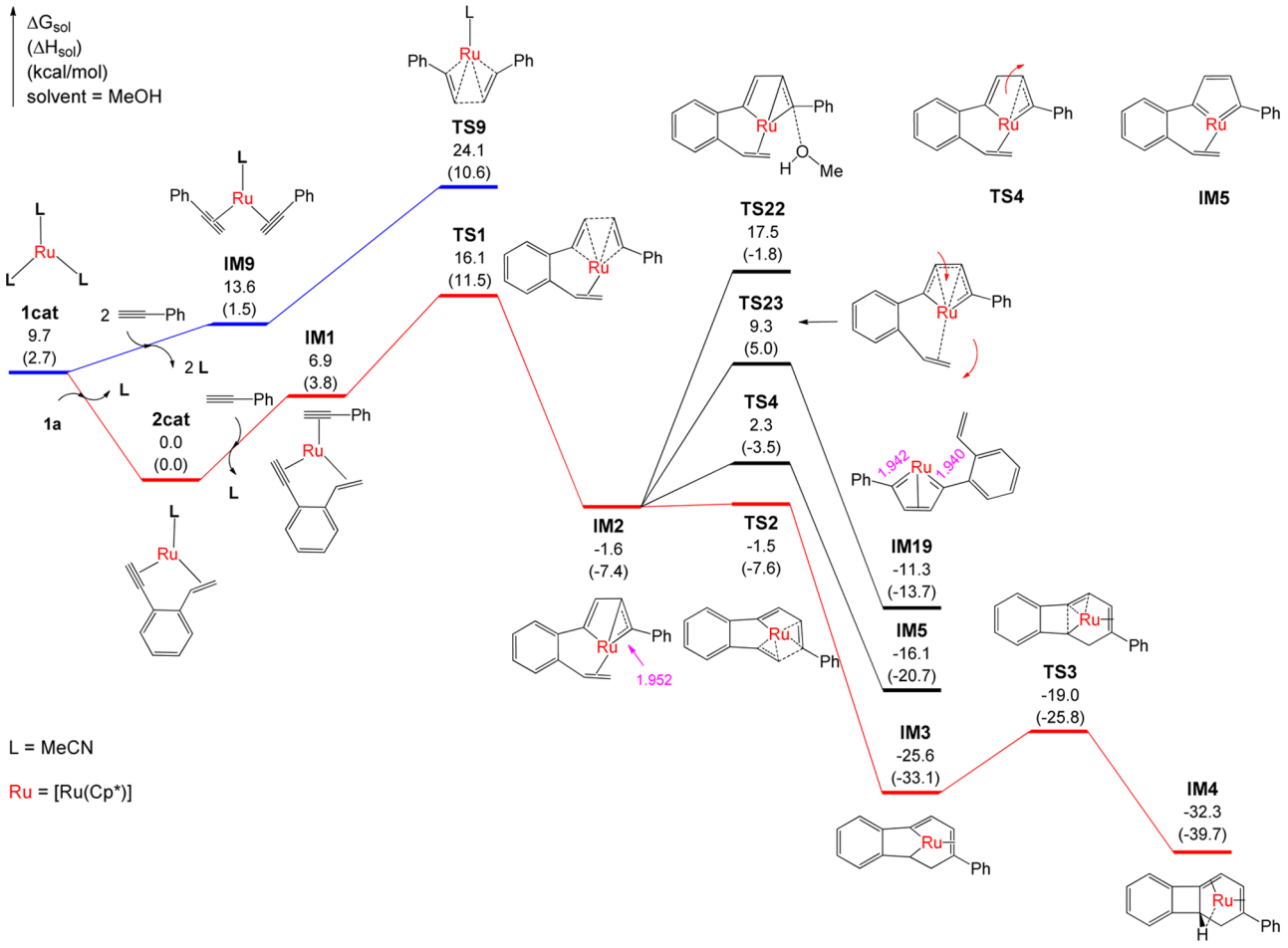

Figure 9. Free energy profiles for Ru-catalyzed [2 + 2 + 2] cycloaddition of **1a** with **2a** and pathways leading to 1,3-dienyl ether. Energies are relative to **2cat** and are mass balanced.

As the discussion above excludes eq 3 in system 2, we further quested if **IM2** can promote an eq 3-like reaction in system 2, and we examined if **IM2** is able to react with methanol via mechanisms described in Figures 6 and 7 to give **3b**-like product. **TS22** describes the methanol nucleophilic attack at **IM2**. Because the attacked C^1 (Q = 0.282e) in **IM2** is less electrophilic than its counterpart C^α (Q = 0.315e) in **IM10**, the barrier (19.1 kcal/mol) for the methanol attack at **IM2** is higher than the 13.7 kcal/mol for the attack at **IM10**. The barrier (19.1 kcal/mol) is not high and experimentally accessible. Nevertheless, **TS22** is much higher (19.0 kcal/mol) than **TS2**, which turns off the reaction of **IM2** with methanol. The reactions of methanol with **IM5** and **IM19** can also be singled out, because (i) the TSs (**TS4** for forming **IM5** and **TS23** for **IM19**) are higher than **TS2** and (ii) the resulting **IM5** and **IM19** are already higher than **TS3** for reductive elimination.

On the basis of the above discussion, we conclude that (i) the chemoselectivity of **2b** (eq 2) over **3b** (eq 3) in system 2 is because the chelation of **1a** suffers less entropy penalty than the coordinations of two separate **2a** molecules, and (ii) the reasons for not producing **3b**-like product in system 2 is that the intramolecular *distal*-alkene migratory insertion in **IM2** and the reductive elimination via **TS3** are too facile, which switches off the reactions of methanol with **IM2** and their isomers (**IM5** and **IM19**). The conclusion (ii) applies to system 1 for not producing **3b**-like product in system 1, because the **1a** dimerizaton (eq 1) has energetics close to that of the cocyclization of **1a** and **2a** (see Figure 4).

3.3. Further Discussion on the Role of IM2/IM10 Intermediate in Equation 2/3. TM-catalyzed [2 + 2 + 2] cycloadditions have been studied extensively.[2−6] Scheme 4 depicts a general mechanism for this class of reactions, which involve **IMA** (a classical alkyne−alkyne oxidative cyclization intermediate, exemplified by **IMA**′ and **IMA**″[19h]) or **IMB** [a bis(carbene) intermediate, represented by **IMB**′]. The ruthenacyclopentatriene **IMB**′ formed via alkyne(**2a**)−alkyne(**2a**) oxidative coupling mediated by neutral RuCp*Cl(COD) complex was crystallized experimentally.[26] Previous computational studies often suggested that **IMB** complex is the key intermediate in the neutral RuCp*Cl-mediated [2 + 2 + 2] cycloadditions.[4] Recently, Yamamoto and Severin groups located **IMC** or **IMC**-like species in their computed pathways.[4j,2Sc] For the [2 + 2 + 2] cycloaddition catalyzed by cationic Ru catalyst, using truncated substrate (acetylene) and catalyst ([RuCp(MeCN)$_3$]$^+$), Kirchner group reported a mechanism involving **IMB** but not **IMC**.[4d] Our computed cationic **IM2** and **IM10** are similar to the *neutral* **IMC** but play much more crucial role to complete the reactions, as discussed below.

For the purpose of clear comparisons, Scheme 5 extracts the key results in Sections 3.1 and 3.2, which are relevant to the discussion below.[27] Different from the general mechanism, our computations confirm that the intermolecular alkyne−alkyne

dx.doi.org/10.1021/jo501399x | J. Org. Chem. 2014, 79, 9046−9064

Scheme 4. Schematic [2 + 2 + 2] Reaction Mechanism with M = Transition Metal

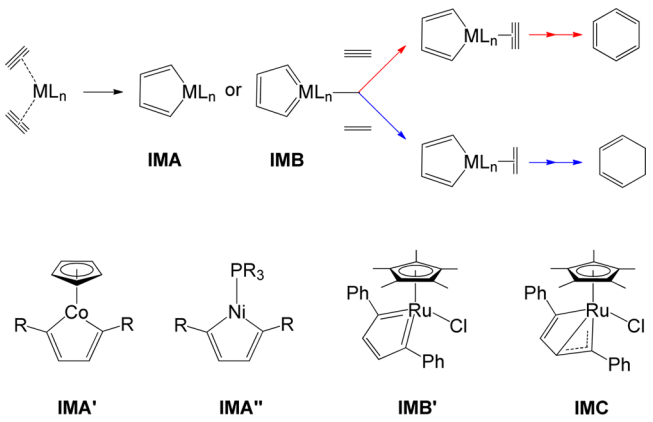

coupling via **TS1**/**TS9** in eq 2/3 directly leads to **IM2**/**IM10** (Figures 1 and 6) rather than either **IMA**- or **IMB**-like intermediates in Scheme 4. It requires passing through a TS (**TS4**/**TS10**) to reach the **IMB**-like intermediate **IM5**/**IM11**. The differences between **IM2**/**IM10** and **IM5**/**IM11** are clearly shown by their geometric differences including (i) the ruthenapentacycle in **IM2**/**IM10** is ruffled, while the metallacycle in **IM5**/**IM11** is planar; (ii) **IM2**/**IM10** features a Ru−C^2 bond with bond length of 2.229/2.218 Å, while no such a bond exists in **IM5**/**IM11** (the Ru···C^2 and Ru···C^3 distances are longer than 2.9 Å); (iii) the bond length difference of Ru−C^1 and Ru−C^4 in **IM2**/**IM10** (0.105/0.194 Å) is larger than that (0.040/0.006 Å) in **IM5**/**IM11**. The NBO charges (Scheme 5A) indicate that C^1 bears larger positive charge than C^4 in **IM2**/**IM10**, while the two carbon atoms in **IM5**/**IM11** are almost equally positive charged. The geometries and charge

Scheme 5. (A) NBO Charges in IM2/IM5 and IM10/IM11; (B and C) Resonance Structures Characterizing IM2/IM10 to Lead to Three Isomerization Channels, along with Key Bond Distances Given in angstroms (Å)

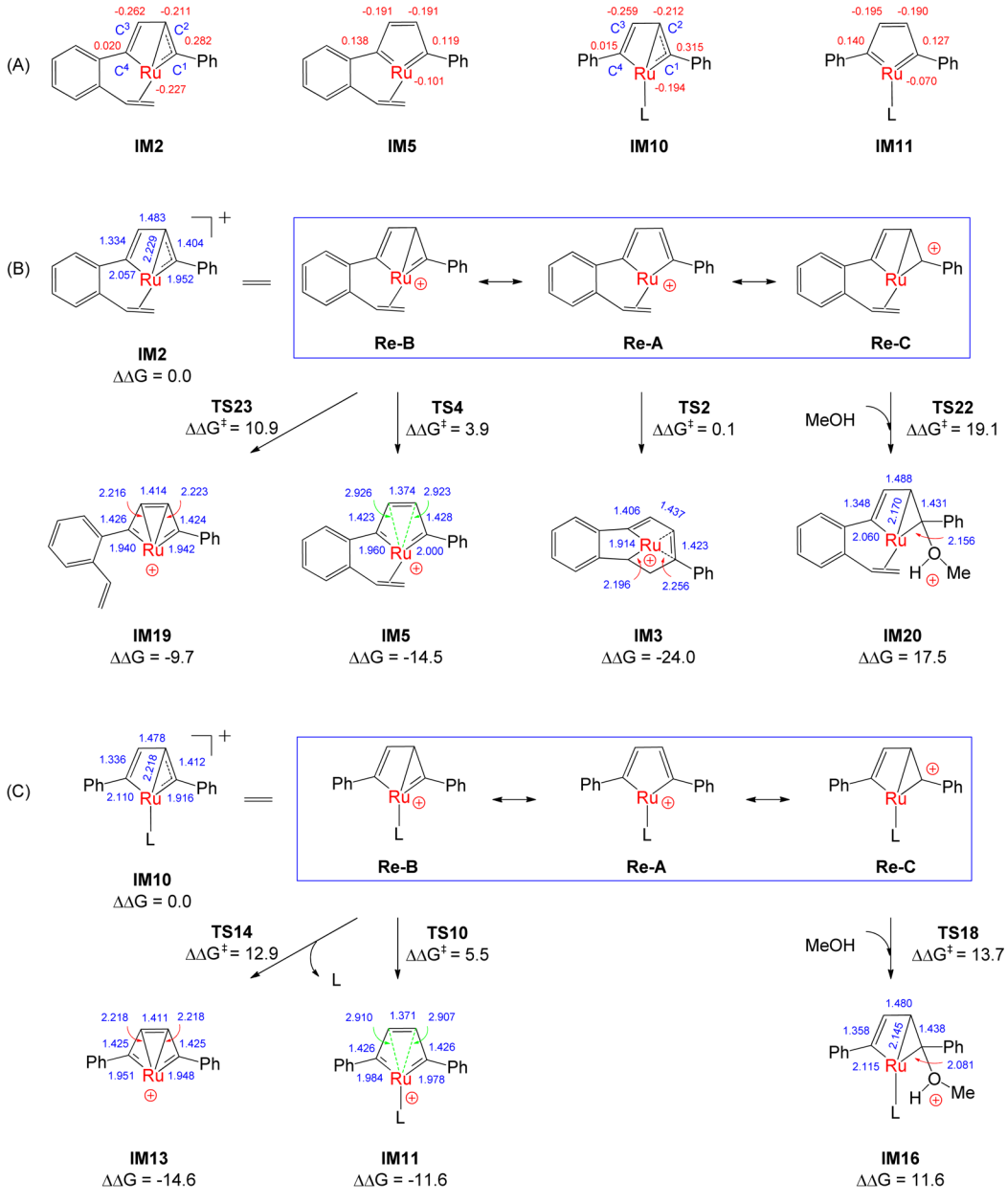

dx.doi.org/10.1021/jo501399x | J. Org. Chem. 2014, 79, 9046−9064

populations of **IM2**/**IM10** and **IM5**/**IM11** suggest that **IM2**/**IM10** can be considered as a Fischer carbene-like mono(carbene), and **IM5**/**IM11** as a Fischer carbene-like bis(carbene).

In the mechanism for the reaction of terminal alkynes (ArC≡CH) with carboxylic acids (RCO_2H) to produce dienylesters, catalyzed by the neutral RuCp*Cl(COD) complex, **IMC** (similar to **IM2**/**IM10**) isomerizes to **IMB′** (similar to **IM5**/**IM11**) which reacts with carboxylic acids to produce dienylester.[25c] Differently, the pathway directly leading **IM5**/**IM11** to final product (**2b**/**3b**) is not energetically favorable in the present cationic catalyst system. In the case of eq 2, the barrier (3.9 kcal/mol) for transformation (**IM2** → **TS4** → **IM5**) is low, but the barrier for intramolecular *proximal*-insertion of C^5═C^6 to Ru−C^4 in **IM5** via **TS5** is prohibitively high (54.1 kcal/mol, see Figure 1). There is a more favorable pathway to transform **IM2** to **IM3** via **TS2**, **IM3** then undergoing reductive elimination to produce **2b**. In the case of eq 3, the transformation of **IM10** → **TS10** → **IM11** is even most favorable, but the reaction barriers of methanol with **IM11** by passing **TS11**−**13** are also high (>34.8 kcal/mol) and substantially higher than that (ca. 25.0 kcal/mol) for the predicted favorable pathways (see Figures 6 and 7).

To account for the various reaction channels starting from **IM2**/**IM10**, based on the geometric and electronic structure of **IM2**/**IM10**, we introduce three resonance structures (**Re-A**, **Re-B**, and **Re-C**, see Scheme 5B,C) to characterize the reactivity properties of the intermediate. The reasonability for the proposal is supported by the optimized structure of **IM2**/**IM10**. Using **IM2** as a representative, we narrate the relevance between resonance structures and geometry. The Ru−C^1 partial double bond (1.952 Å) and C^3═C^4 double bond (1.334 Å) are shorter than the Ru−C^4 single bond (2.057 Å) and C^2−C^3 single bond (1.48 Å), respectively; the C^1−C^2 partial double bond length (1.404 Å) is between that of the C^3═C^4 double bond and that of C^2−C^3 single bond, and the Ru−C^2 is a partial single bond with a bond length of 2.229 Å larger than that of Ru−C^4 single bond (2.057 Å). **Re-A** addresses the characteristic of the regular alkyne−alkyne oxidative coupling intermediate (i.e., **IMA** in Scheme 4), **Re-B** corresponds to the Fischer mono(carbene) characteristic of **IM2**, and **Re-C** characterizes the electrophilicity of **IM2** with a large positive charge (+0.282*e*) on C^1 center. The properties of **IM2** characterized by the three resonance structures play roles to gear three reaction channels. Inserting C^5═C^6 in the Ru−C^1 through **Re-A** results in **IM3**. The cleavage of Ru−C^2 bond through **Re-B** planarizes the ruthenapentacycle, resulting in bis(carbene) **IM5**. The transformation turns formal C^2−C^3 and Ru−C^4 single and C^3═C^4 double bonds to formal C^2═C^3 and Ru═C^4 double and C^3−C^4 single bonds, but maintains the formal Ru═C^1 double bond. The alternations between double and single bonds are reflected by the changing trends of these bond lengths from **IM2** and **IM5** (see Scheme 5B). The ruthenapentacycle in **IM5** contains three formal double bonds and thus can be considered as an aromatic 5-ring, which is indicated by the somewhat bond equalization; the C^1−C^2 and C^3−C^4 bonds have lengths (1.423 and 1.428 Å, respectively), which are between those of regular C−C single bond (1.500 in ethane) and C═C double bond (1.339 Å in ethene), and the C^2═C^3 bond is longer than the regular C═C double bond. The aromaticity of **IM5** contributes to the weak reactivity of the complex, as reflected by the high barrier (54.1 kcal/mol) between **IM5** and **TS5** in Figure 1, in addition to the contribution due to the strained 4-ring in **TS5**. Interestingly, the breaking of Ru−C^2 bond can also lead to another bis(carbene) (**IM19**). The ruthenapentacycle in **IM5** is planar and the newly created C^2═C^3 double bond does not coordinate to Ru center. Alternatively, the metallacycle can fold, enabling the newly formed C^2═C^3 double bond to coordinate to Ru center, which meantime pushes the prior coordinated alkene (C^5═C^6) group away to avoid coordinative and electronic oversaturation on Ru-center, resulting in **IM19**.

The above discussions on **IM2** isomerizations in eq 2 can be applied to understand the transformations from **IM10** to **IM11**, **IM13**, and **IM16** in eq 3, respectively, and the reactivities of these complexes (Scheme 5C). **IM11** due to **Re-B** possess an aromatic ruthenapentacycle; thus, the various H-transfers from methanol to the aromatic 5-ring have high barrier (see Figure 6). Different from **IM19** in which the dissociated alkene group still exists, the MeCN ligand is completely liberated during the transformation from **IM10** to **IM13**; however, **IM13** is similar to **IM19** in terms of electronic structure. Among the two bis(carbene) species (**IM5** and **IM19**, Scheme 5B), the aromatic **IM5** is 4.8 kcal/mol more stable than the nonaromatic **IM19**, while the aromatic **IM11** is 3.0 kcal/mol less stable than the nonaromatic **IM13**. The latter seems signify a discrepancy with the aromaticity stabilization effect. However, we call attention to that the relative energies are estimated in terms of free energy. The process from **IM10** to **IM13** dissociates a MeCN ligand completely, thus benefiting from the entropy contribution, whereas the transformation from **IM10** to **IM11** is a unimolecular isomerization without gaining similar entropy contribution. In terms of enthalpy, **IM11** is 9.2 kcal/mol more stable than **IM13** (Figure 6), and the value is compared with the 7.0 kca/mol difference between **IM5** and **IM19** (Figure 9). Because **IM13** is nonaromatic but still features an electrophilic center, it is susceptible to methanol nucleophilic attack, opening a feasible pathway leading to product **3b** (Figure 6). **Re-C** characterizes the electrophilic property of **IM10** itself; thus, a nucleophile (e.g., methanol as in eq 3) can attack the electrophilic center (C^1) with a barrier of 13.7 kcal/mol, resulting in **IM16** which then transforms to **3b** (Figure 7). In agreement with our proposal that the aromaticity contributes to the weak reactivity of **IM11**, both **IM10** and **IM13** that lead to feasible methanol nucleophilic attack pathways are nonaromatic. Similarly, **IM2** is also susceptible to the methanol nucleophilic attack via **TS22** (Figure 9); the barrier (19.1 kcal/mol) is not high, but much less competitive with the [2 + 2 + 2] cycloaddition pathway, as discussed in Section 3.2.

3.4. [2 + 2 + 2] Cycloaddition versus Aromatization.

3.4.1. Aromatization Mechanism for Equation 4 Reaction. Aromatization of **1a** to give naphthalene is thermodynamically downhill by 54.2 kcal/mol (vide infra). Using a different **Ru2** ($[Ru(Tp)(PPh_3)(MeCN)_2]PF_6$), Liu et al. have realized the process (eq 4).[14] It has been assumed that the electrocyclization of aromatic enynes involved a metal vinylidene complex.[14,28] To understand how the different catalysts (**1cat** vs **3cat**) control the productions of **1b** and **4b** (cycloaddition vs aromatization), respectively, we explored various pathways for the **3cat**-catalyzed aromatization leading **1a** to **4b** (Supporting Information Scheme S3). The most favorable one is presented in Figure 10 with the key structures displayed in Figure 11.

The aromatization of **1a** begins by replacing a liable MeCN ligand with substrate **1a**, giving an 18*e* π-complex **IM21** at energetic cost of 11.8 kcal/mol. Subsequently, a 1,2-H transfer described by **TS24** transforms **IM21** to a Ru−vinylidene

dx.doi.org/10.1021/jo501399x | J. Org. Chem. 2014, 79, 9046−9064

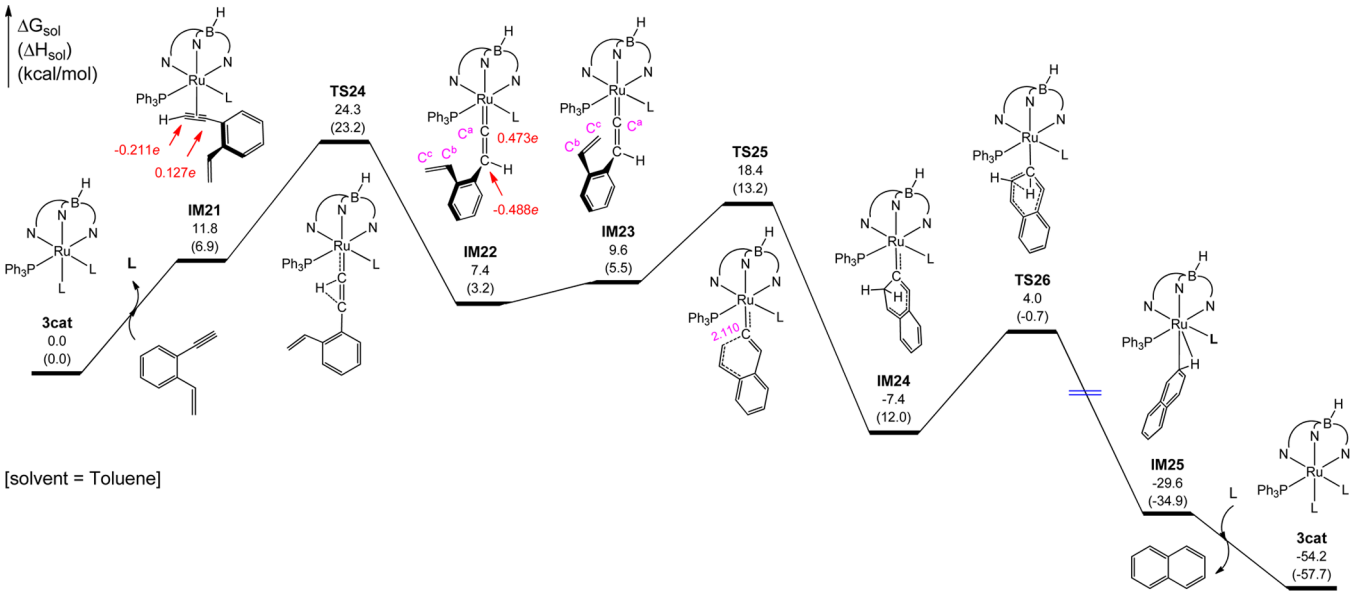

Figure 10. Free energy profiles for the **3cat**-catalyzed aromatization of *ortho*-ethynylstyrene **1a**. Energies are relative to **3cat** + **1a** and are mass balanced.

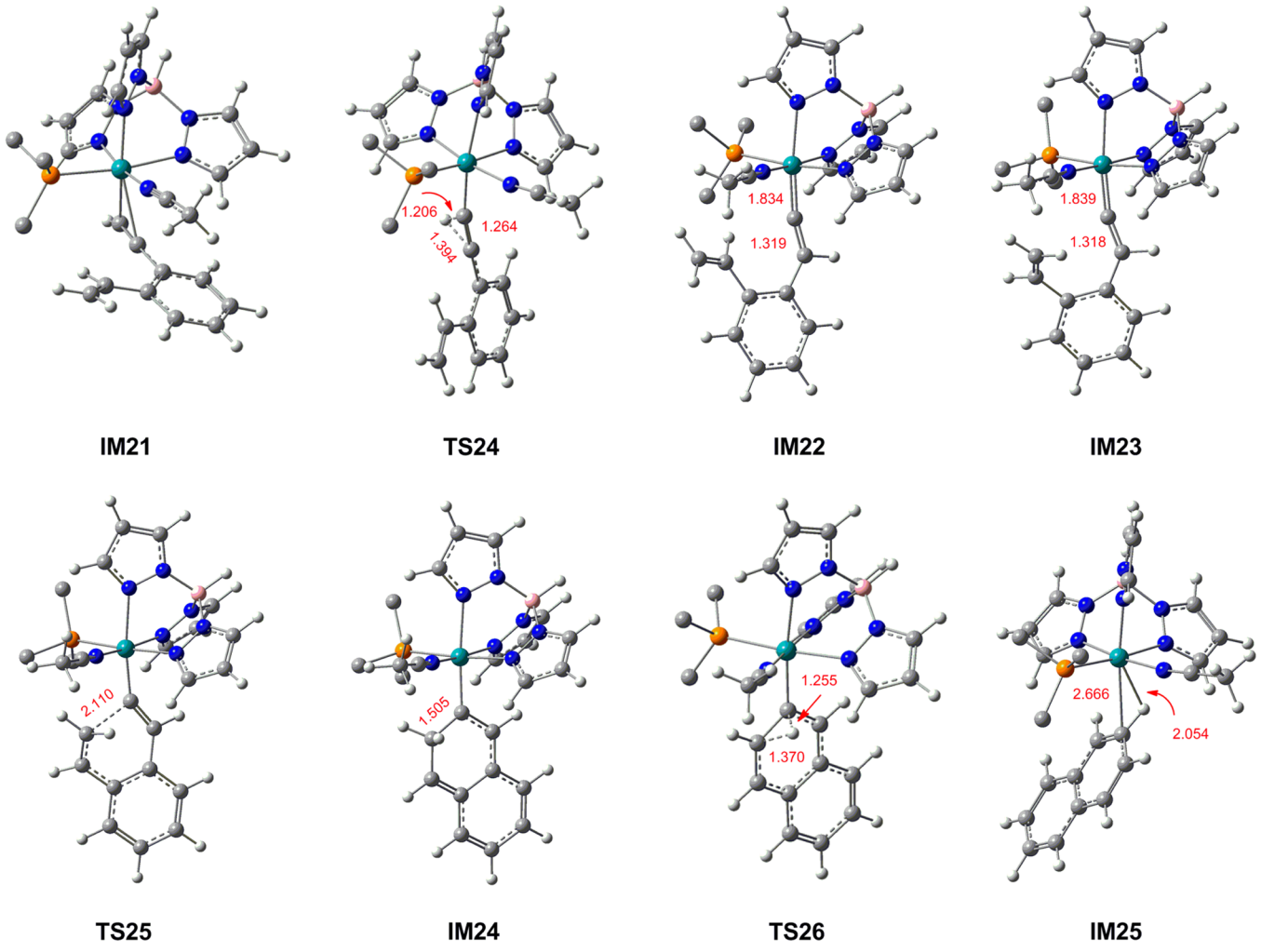

Figure 11. Key structures for **3cat**-catalyzed aromatization of *ortho*-ethynylstyrene (**1a**), with selected bond distances given in angstroms (Å). Phenyl groups of the PPh_3 ligand are omitted for clarity.

dx.doi.org/10.1021/jo501399x | J. Org. Chem. 2014, 79, 9046−9064

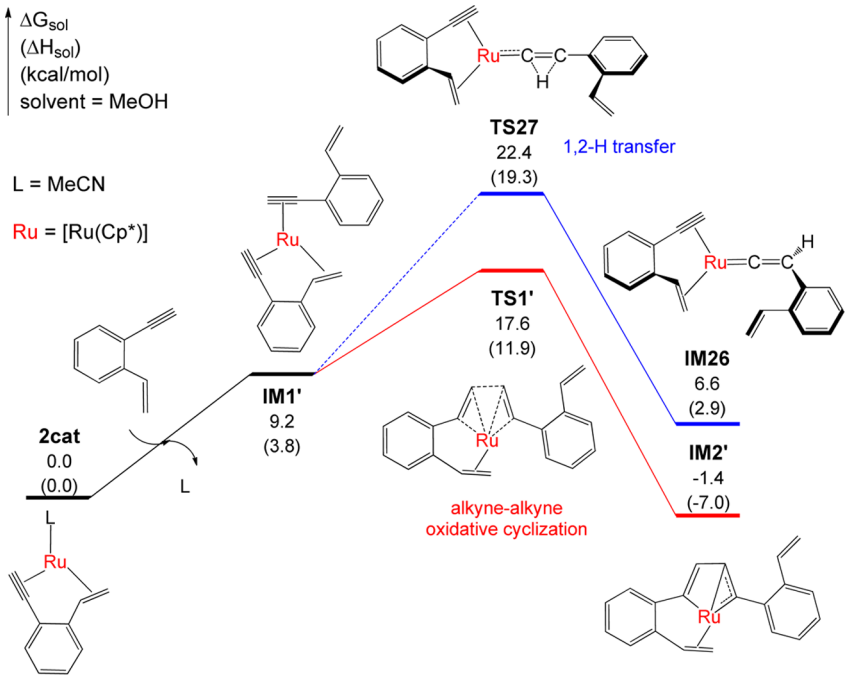

Figure 12. Free energy profiles for **2cat**-catalyzed [2 + 2 + 2] dimerization vs aromatization of *ortho*-ethynylstyrene **1a**. Energies are relative to **2cat** + **1a** and are mass balanced.

intermediate **IM22**.[29−31] The terminal alkyne-to-vinylidene isomerization reverses the polarities of C^{α} and C^{β},[29] as shown by the changes of NBO charges on C^{α} and C^{β} from **IM21** to **IM22** in Figure 10. The polarity reverse makes C^{α} electrophilic and susceptible to nucleophilic attack. In **IM22**, the charges on C^{a} (+0.473*e*), C^{b}(−0.193*e*), and C^{c} (−0.368*e*) suggest that the $C^{a}\cdots C^{c}$ bond formation should be preferred via nucleophilic attack of C^{c} at C^{a}, which also agrees with the preference of forming a 6-ring over 5-ring. In **IM22**, the C^{c} atom is 4.092 Å apart from C^{a}, geometrically improper for the $C^{a}-C^{c}$ bond formation; thus, **IM22** isomerizes to **IM23** to make C^{c} proximal to C^{a} [$R(C^{a}-C^{c})$ = 3.034 Å] to facilitate the nucleophilic attack. The attack is enabled via **TS25** and leads to the Ru−naphthylidene complex **IM24**. Relative to **IM23**, the process crosses a barrier of 8.8 kcal/mol and is downhill by 17.0 kcal/mol. Subsequently, another 1,2-H shift drives **IM24** down to **IM25** [a Ru-η^2(C−H)−naphthalene complex]. The mechanism for isomerization of **IM24** to **IM25** is similar to the classical mechanism transforming a methyl substituted carbene to a metal-olefin species.[32] Replacement of the naphthalene moiety in **IM25** with a MeCN ligand liberates the naphthalene product **4b** and regenerates the catalyst **3cat**. Taking the whole pathway into account, the rate-determining step is the first 1,2-H transfer via **TS24** with an energy barrier of 24.3 kcal/mol, and the transformation is highly exergonic by 54.2 kcal/mol. The pathway in Figure 10 only dissociates one MeCN ligand. We also explored the scenarios which dissociate two MeCN ligands from **3cat**. However, as shown in Supporting Information Scheme S3, the pathways have rate-determining barriers (>40 kcal/mol) much higher than **TS24**, because the intermediates and TSs in Figure 10 maintain optimal coordination mode (see Figure 11), meeting the 18*e*-rule, having six coordinations with octahedral arrangements.

3.4.2. Origins for the Selectivity between [2 + 2 + 2] Cycloaddition and Aromatization. On the basis of the mechanism for the aromatization of **1a** to **4b** catalyzed by **3cat**, we now understand why the aromatization (eq 4) did not operate in the system 1. Because the 1,2-H transfer via **TS24** (Figure 12) is a rate-determining step, we only considered the 1,2-H-transfer pathway for **2cat**-catalyzed aromatization of **1a**, as shown in Figure 12 (the full catalytic cycle is given in Supporting Information Figure S3). **TS27** is the rate-determining 1,2-H transfer TS, corresponding to **TS24** in Figure 9. The barrier for the 1,2-H transfer is 22.4 kcal/mol relative to **2cat** + **1a**, which is even smaller than the 1,2-H transfer barrier of 24.2 kcal/mol (**TS24** relative to **3cat** +**1a**) for eq 4 (an experimentally realized reaction). However, the 1,2-H transfer barrier (22.4 kcal/mol, **TS27**) is higher than the oxidative coupling barrier (17.6 kcal/mol, **TS1′**) leading to **1b**. Therefore, the origin for choosing [2 + 2 + 2] dimerization of **1a** in system 1 is not because the aromatization route is energetically inaccessible, but because the dimerization process is more favorable.

Reversely, we further investigated why the [2 + 2 + 2] dimerization (eq 1) did not occur in Liu et al.'s system 4 by focusing on the rate-determining oxidative coupling step. In the TS optimizations, we considered various coordination modes of **1a** to Ru center via replacing 2*MeCN, MeCN + PPh_3, 2*MeCN + PPh_3, respectively, and coupling modes via the alkyne−alkyne and alkyne−alkene couplings in either head-to-head or head-to-tail manner (Supporting Information Scheme S4). Among the TSs of different scenarios, Figure 13 shows representatives (**TS28**, **TS29**, and **TS30**) which exemplify the scenarios of **1a** substitution for 2*MeCN, MeCN + PPh_3, and 2*MeCN + PPh_3, respectively. The high barriers corroborate that the [2 + 2 + 2] dimerization of **1a** could not occur in system 4, which produced **4b** via aromatization selectively. The high barriers can be understood in terms of the geometric and electronic structures of the TSs in Figure 13. If the PPh_3 ligand remains, as described by **TS28**, the coupling causes severe steric

dx.doi.org/10.1021/jo501399x | J. Org. Chem. 2014, 79, 9046−9064

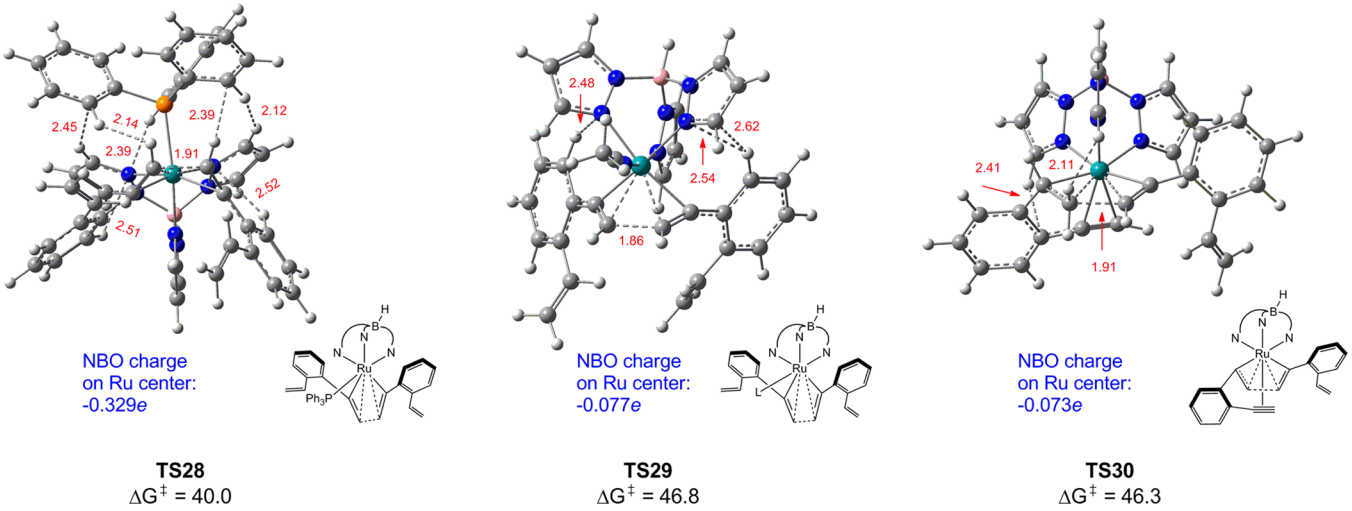

Figure 13. Optimized geometries and activation energies for the oxidative coupling TSs **TS28**, **TS29**, and **TS30**, with selected bond distances given in angstroms (Å). Energies are relative to **3cat** and are mass balanced.

hindrance among Tp, PPh_3, and **1a** substrate. If the PPh_3 ligand is substituted, as exemplified by **TS29** and **TS30**, because of the loss of strong electron-donating PPh_3 ligand, the negative charge on Ru center decreases significantly (from −0.329 to −0.077 to −0.073*e*), which disfavors the oxidative processes, explaining why the **TS29** and **TS30** even have higher barrier than **TS28**, though they suffer steric hindrance less severely than **TS28**.

4. CONCLUSIONS

In conclusion, we have performed a detalied computational study to understand the catalytic mechanisms of the four experimentally realized reactions (eqs 1−4) occurring in the four systems (systems 1−4), as well as the chemo- and regioselectivities involved in these systems.

For eq 2, after generating the active catalyst **2cat**, the reaction procceds via three major stages including oxidative coupling, migratory insertion, and reductive elimination, in which the oxidative coupling is the rate-determining step in the full catalytic cycle. Among the three possible oxidative coupling modes (CMA, CMB, and CMC in Scheme 2), the CMA mode (intermolecular alkyne−alkyne coupling) is more favorable than others by at least 3.5 kcal/mol. Of the *distal*- and *proximal*-alkene migratory insertion modes, the *distal*-insertion pathway is preferred.

Equation 1 follows a similar mechanism. The oxidative coupling step for this reaction is also accessible, but less favorable than that in eq 1, explaining why eq 1 did not occur in in system 2. The causes for not producing the regioisomers (**1b−r** and **2b−r**) are becasue (i) the groups beared on the two carbon atoms coupling together result in severe steric hindrance between substrates and substrates/catalyst, and (ii) the steric hindrance distorts the π-conjugation betwen benzene ring and the C═C π bond of the coupling substrate, which destabilize the coupling TSs.

Equation 3 takes place via three stages including oxidative coupling, methanol nucleophilic attack, and hydrogen transfer. The oxidative coupling step is similalr to that in eqs 1 and 2. The oxidative coupling step leads to an intermediate (**IM10**) which then isomerizes to **IM13**. Both **IM10** and **IM13** feature electrophilic carbon center for methanol nucleophilc attack, leading to two pathways to give 1,3-dienyl ether. The two pathways are experimentally accessible and energetically comparable. The reason for the reaction channel not occurring in system 1/2 is because the alkene migratory *distal*-insertion with a 2.6/0.1 kcal/mol barrier (see **TS2′**/**TS2** in Figure 1/4, respectively) is extremely easy, which gears **IM2′**/**IM2** to **IM3′**/**IM3** for reductive elimination, affording product **1b**/**2b**. The reductive elimination barriers are less than 7.0 kcal/mol. The mechanism via directly transferring methanol hydroxyl H to the C^{α} of **IM11**, which is similar to the reaction of terminal alkynes with carboxylic acids catalyzed by the neutral RuCp*Cl(COD) complex, is not feasible in this cationic catalytic system. The mechanistic difference between the two systems can be attributed to the fact that proton in carboxylic acid is more acidic than that in methanol.

Equation 4 undergoes, via three major stages after **1a** coordination to **3cat** via ligand dissociation, including the formation of a Ru−vinylidene intermediate (**IM22**) via 1,2-H transfer, intramolecular nucleophilic attack to close the 6-ring and form the C−C bond, and 1,2-H shift to a Ru-η^2(C−H)−naphthalene complex (**IM25**) via an isomerization similar to the classical mechanism of transforming a methyl substituted carbene to a metal-olefin species. The first stage of 1,2-H transfer process is the rate-determining step. Equation 4 reaction did not occur in systems 1 and 2 because the barrier for forming the Ru−vinylidene complex is higher than the oxidative coupling barrier. Equation 1 reaction did not occur in system 4 because the coupling barrier for dimerization is prohibitive (>38.0 kcal/mol) due to sterically demanding catalysts.

We call particular attention to the important role of the chameleon-like species (**IM2** in eq 2 and **IM10** in eq 3, see Scheme 5) formed directly via intermolecular alkyne−alkyne oxidative couplings. Their geometric and electronic structures suggest that their reactivity properties could be characterized by three resonance structures (**Re-A**, **Re-B**, and **Re-C**). **Re-A** describes the features of the classical intermediates involved in the alkyne−alkene oxidative couplings, **Re-B** characterizes the mono(carbene) characteristic of the intermediates, and **Re-C** represents the electrophilicity of the intermediates. The properties characterized by the three resonance structures open three channels to give isomers for subsequent reaction steps. Interestingly, the bis(carbene) intermediates (**IM5** and **IM11**) due to **Re-B**, which are similar to the bis(carbene)

dx.doi.org/10.1021/jo501399x | J. Org. Chem. 2014, 79, 9046−9064

intermediates generally considered to be crucial in the neutral RuCp*Cl-catalyzed systems, could be accessed feasibly, but they are not reactive enough for the subsequent reaction steps. The aromaticity of these complexes (**IM5** and **IM11**) (partially) contributes their loss of reactivity. The intermediates (nonaromatic **IM3** and **IM13** through **Re-A** and **Re-B**, respectively) continue the subsequent steps. In addition, **IM2**/**IM10** features an electrophilic center (characterized by **Re-C**) and is susceptible to the attack of nucleophiles (e.g., methanol). These findings may help to understand not only the four specific reactions but also for the general [2 + 2 + 2] cycloaddition.

■ ASSOCIATED CONTENT

Supporting Information

Additional computational results and complete ref 16. This material is available free of charge via the Internet at http://pubs.acs.org.

■ AUTHOR INFORMATION

Corresponding Author

*E-mail: zxwang@ucas.ac.cn

Notes

The authors declare no competing financial interest.

■ ACKNOWLEDGMENTS

This work is financially supported by National Natural Science Foundation of China (Nos. 21173263 and 21373216).

■ REFERENCES

(1) Selected reviews on transition-metal-catalyzed cycloadditions: (a) Lautens, M.; Klute, W.; Tam, W. *Chem. Rev.* **1996**, *96*, 49. (b) Ojima, I.; Tzamarioudaki, M.; Li, Z.; Donovan, R. J. *Chem. Rev.* **1996**, *96*, 635. (c) Yet, L. *Chem. Rev.* **2000**, *100*, 2963. (d) Aubert, C.; Buisine, O.; Malacria, M. *Chem. Rev.* **2002**, *102*, 813. (e) Nakamura, I.; Yamamoto, Y. *Chem. Rev.* **2004**, *104*, 2127. (f) Rubin, M.; Rubina, M.; Gevorgyan, V. *Chem. Rev.* **2007**, *107*, 3117. (g) Gulevich, A. V.; Dudnik, A. S.; Chernyak, N.; Gevorgyan, V. *Chem. Rev.* **2013**, *113*, 3084.

(2) Recent reviews for transition-metal-catalyzed [2 + 2 + 2] cycloadditions, see: (a) Agenet, N.; Buisine, O.; Slowinski, F.; Gandon, V.; Aubert, C.; Malacria, M. Cotrimerizations of Acetylenic Compounds. In *Organic Reactions*; RajanBabu, T. V., Ed.; John Wiley and Sons: Hoboken, NJ, 2007; Vol. *68*, p 1. (b) Saito, S.; Yamamoto, Y. *Chem. Rev.* **2000**, *100*, 2901. (c) Varela, J. A.; Saá, C. *Chem. Rev.* **2003**, *103*, 3787. (d) Nakamura, I.; Yamamoto, Y. *Chem. Rev.* **2004**, *104*, 2127. (e) Henry, G. D. *Tetrahedron* **2004**, *60*, 6043. (f) Yamamoto, Y. *Curr. Org. Chem.* **2005**, *9*, 503. (g) Kotha, S.; Brahmachary, E.; Lahiri, K. *Eur. J. Org. Chem.* **2005**, 4741. (h) Chopade, P. R.; Louie, J. *Adv. Synth. Catal.* **2006**, *348*, 2307. (i) Gandon, V.; Aubert, C.; Malacria, M. *Chem. Commun.* **2006**, 2209. (j) Tanaka, K. *Synlett* **2007**, 1977. (k) Agenet, N.; Buisine, O.; Slowinski, F.; Gandon, V.; Aubert, C.; Malacria, M. *Org. React.* **2007**, *68*, 1. (l) Heller, B.; Hapke, M. *Chem. Soc. Rev.* **2007**, *36*, 1085. (m) Shibata, T.; Tsuchikama, K. *Org. Biomol. Chem.* **2008**, *6*, 1317. (n) Galan, B. R.; Rovis, T. *Angew. Chem., Int. Ed.* **2009**, *48*, 2830. (o) Perreault, S.; Rovis, T. *Chem. Soc. Rev.* **2009**, *38*, 3149. (p) Broere, D. L. J.; Ruijter, E. *Synthesis* **2012**, *44*, 2639.

(3) Reppe, W.; Schweckendiek, W. J. *Justus Liebigs Ann. Chem.* **1948**, *560*, 104.

(4) Theoretical studies on transition-metal-catalyzed [2 + 2 + 2] cycloadditions: (a) Kirchner, K.; Calhorda, M. J.; Schmid, R.; Veiros, L. F. *J. Am. Chem. Soc.* **2003**, *125*, 11721. (b) Yamamoto, Y.; Arakawa, T.; Ogawa, R.; Itoh, K. *J. Am. Chem. Soc.* **2003**, *125*, 12143. (c) Yamamoto, Y.; Kinpara, K.; Saigoku, T.; Takagishi, H.; Okuda, S.; Nishiyama, H.; Itoh, K. *J. Am. Chem. Soc.* **2005**, *127*, 605. (d) Ruba, E.; Schmid, R.; Kirchner, K.; Calhorda, M. J. *J. Organomet. Chem.* **2003**, *682*, 204. (e) Schmid, R.; Kirchner, K. *J. Org. Chem.* **2003**, *68*, 8339. (f) Dazinger, G.; Torres-Rodrigues, M.; Kirchner, K.; Calhorda, M. J.; Costa, P. J. *J. Organomet. Chem.* **2006**, *691*, 4434. (g) Dazinger, G.; Schmid, R.; Kirchner, K. *New J. Chem.* **2004**, *28*, 153. (h) Varela, J. A.; Rubín, S. G.; Castedo, L.; Saá, C. *J. Org. Chem.* **2008**, *73*, 1320. (i) Varela, J. A.; Saá, C. *J. Organomet. Chem.* **2009**, *694*, 143. (j) Dutta, B.; Curchod, B. F. E.; Campomanes, P.; Solari, E.; Scopelliti, R.; Rothlisberger, U.; Severin, K. *Chem.—Eur. J.* **2010**, *16*, 8400. (k) Also see refs 5 and 6..

(5) (a) Gandon, V.; Agenet, N.; Vollhardt, K. P. C.; Malacria, M.; Aubert, C. *J. Am. Chem. Soc.* **2006**, *128*, 8509. (b) Agenet, N.; Gandon, V.; Vollhardt, K. P. C.; Malacria, M.; Aubert, C. *J. Am. Chem. Soc.* **2007**, *129*, 8860. (c) Aubert, C.; Gandon, V.; Geny, A.; Heckrodt, T. J.; Malacria, M.; Paredes, E.; Vollhardt, K. P. C. *Chem. −Eur. J.* **2007**, *13*, 7466.

(6) (a) Dahy, A. A.; Koga, N. *Bull. Chem. Soc. Jpn.* **2005**, *78*, 781. (b) Dahy, A. A.; Suresh, C. H.; Koga, N. *Bull. Chem. Soc. Jpn.* **2005**, *78*, 792. (c) Orian, L.; vanStralen, J. N. P.; Bickelhaupt, F. M. *Organometallics* **2007**, *26*, 3816. (d) Yoshikai, N.; Zhang, S.-L.; Yamagata, K.-i.; Tsuji, H.; Nakamura, E. *J. Am. Chem. Soc.* **2009**, *131*, 4099. (e) Dachs, A.; Torrent, A.; Roglans, A.; Parella, T.; Osuna, S.; Solá, M. *Chem.—Eur. J.* **2009**, *15*, 5289. (f) Dachs, A.; Osuna, S.; Roglans, A.; Solá, M. *Organometallics* **2010**, *29*, 562. (g) Guo, C.-H.; Wu, H.-S.; Hapke, M.; Jiao, H. *J. Organomet. Chem.* **2013**, *748*, 29.

(7) (a) Shepherd, M. K. In *Cyclobutadienes: The Chemistry of Benzocyclobutene, Biphenylene and Related Compounds*; Elsevier: Amsterdam, 1991. (b) Sadana, A. K.; Saini, R. K.; Billups, W. E. *Chem. Rev.* **2003**, *103*, 1539. (c) Chaumontet, M.; Retailleau, P.; Baudoin, O. *J. Org. Chem.* **2009**, *74*, 1774.

(8) (a) Tutar, A.; Cakmak, O.; Karakas, M.; Onal, A.; Ide, S. *J. Chem. Res.* **2004**, 545. (b) Hart, H.; Teuerstein, A. *Synthesis* **1979**, 693. (c) Iyoda, M. *Adv. Synth. Catal.* **2009**, *351*, 984. (d) Winkler, M.; Wenk, H. H.; Sander, W. In *Reactive Intermediate Chemistry*; Moss, R. A., Platz, M. S., Jones, M., Eds.; Wiley: Hoboken, NJ, 2004; p 741.

(9) Also see Ru-catalyzed [4 + 2+2] cycloaddition reactions by Saá group: (a) Varela, J. A.; Castedo, L.; Saá, C. *Org. Lett.* **2003**, *5*, 2841. (b) García-Rubín, S.; Varela, J. A.; Castedo, L.; Saá, C. *Org. Lett.* **2009**, *11*, 983. Selected examples of Co-catalyzed [2 + 2 + 2] cycloadditions of *ortho*-diethynylarenes with alkynes: (c) Berris, B. C.; Hovakeemian, G. H.; Lai, Y. H.; Mestdagh, H.; Vollhardt, K. P. C. *J. Am. Chem. Soc.* **1985**, *107*, 5670. (d) Schmidt-Radde, R. H.; Vollhardt, K. P. C. *J. Am. Chem. Soc.* **1992**, *114*, 9713. (e) Han, S.; Anderson, D. R.; Bond, A. D.; Chu, H. V.; Disch, R. L.; Holmes, D.; Schulman, J. M.; Teat, S. J.; Vollhardt, K. P. C.; Whitener, G. D. *Angew. Chem., Int. Ed.* **2002**, *41*, 3227. (f) Bong, D. T. Y.; Chan, E. W. L.; Diercks, R.; Dosa, P. I.; Haley, M. M.; Matzger, A. J.; Miljanic, O. S.; Vollhardt, K. P. C.; Bond, A. D.; Teat, S. J.; Stanger, A. *Org. Lett.* **2004**, *6*, 2249. (g) Iglesias, B.; Cobas, A.; Perez, D.; Guitian, E.; Vollhardt, K. P. C. *Org. Lett.* **2004**, *6*, 3557. (h) Dosa, P. I.; Gu, Z.; Hager, D.; Karney, W. L.; Vollhardt, K. P. C. *Chem. Commun.* **2009**, 1967.

(10) García-Rubín, C.; González-Rodríguez, C.; García-Yebra, C.; Varela, J. A.; Esteruelas, M. A.; Saá, C. *Angew. Chem., Int. Ed.* **2014**, *53*, 1841.

(11) Trost, B. M.; Frederiksen, M. U.; Rudd, M. T. *Angew. Chem., Int. Ed.* **2005**, *44*, 6630.

(12) Zhang, M.; Jiang, H.-F.; Neumann, H.; Beller, M.; Dixneuf, P. H. *Angew. Chem., Int. Ed.* **2009**, *48*, 1681.

(13) Chan, W.-C.; Lau, C.-P.; Chen, Y.-Z.; Fang, Y.-Q.; Ng, S.-M.; Jia, G. *Organometallics* **1997**, *16*, 34.

(14) Shen, H.-C.; Pal, S.; Lian, J. J.; Liu, R.-S. *J. Am. Chem. Soc.* **2003**, *125*, 15762.

(15) The eqs 1−3 could be drawn:

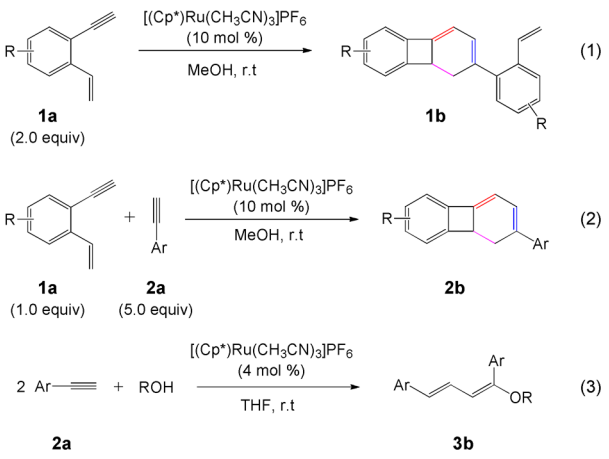

(16) Frisch, M. J. et al. *Gaussian 09*, revision A.01; Gaussian, Inc.: Wallingford, CT, 2009.
(17) Zhao, Y.; Truhlar, D. G. *Theor. Chem. Acc.* **2008**, *120*, 215.
(18) (a) Zhao, Y.; Truhlar, D. G. *Acc. Chem. Res.* **2008**, *41*, 157. (b) Zhao, Y.; Truhlar, D. G. *J. Chem. Theory Comput.* **2009**, *5*, 324. (c) Kulkarni, A. D.; Truhlar, D. G. *J. Chem. Theory Comput.* **2011**, *7*, 2325.
(19) The M06 functional is optimized with a particular focus on organometallic systems and has been used successfully in earlier studies, see: (a) Benitez, D.; Shapiro, N. D.; Tkatchouk, E.; Wang, Y. M.; Goddard, W. A., III; Toste, F. D. *Nat. Chem.* **2009**, *1*, 482. (b) Benitez, D.; Tkatchouk, E.; Goddard, W. A., III. *Organometallics* **2009**, *28*, 2643. (c) Sieffert, N.; Bühl, M. *Inorg. Chem.* **2009**, *48*, 4622. (d) Ariafard, A.; Hyland, C. J. T.; Canty, A. J.; Sharma, M.; Yates, B. F. *Inorg. Chem.* **2011**, *50*, 6449. (e) Bantreil, X.; Prestat, G.; Moreno, A.; Madec, D.; Fristrup, P.; Norrby, P.-O.; Pregosin, P. S.; Poli, G. *Chem.—Eur. J.* **2011**, *17*, 2885. (f) Makarov, I. S.; Fristrup, P.; Madsen, R. *Chem.—Eur. J.* **2012**, *18*, 15683. (g) Xu, L.; Zhu, Q.; Huang, G.; Cheng, B.; Xia, Y. *J. Org. Chem.* **2012**, *77*, 3017. (h) Komagawa, S.; Wang, C.; Morokuma, K.; Saito, S.; Uchiyama, M. *J. Am. Chem. Soc.* **2013**, *135*, 14508. (i) Xu, L.; Hilton, M. J.; Zhang, X.; Norrby, P.-O.; Wu, Y.-D.; Sigman, M. S.; Wiest, O. *J. Am. Chem. Soc.* **2014**, *136*, 1960.
(20) (a) Andrae, D.; Häussermann, U.; Dolg, M.; Stoll, H.; Preuss, H. *Theor. Chim. Acta* **1990**, *77*, 123. (b) Roy, L. E.; Hay, P. J.; Martin, R. L. *J. Chem. Theory Comput.* **2008**, *4*, 1029.
(21) Marenich, A. V.; Cramer, C. J.; Truhlar, D. G. *J. Phys. Chem. B* **2009**, *113*, 6378.
(22) (a) Jiao, L.; Lin, M.; Yu, Z.-X. *J. Am. Chem. Soc.* **2011**, *133*, 447. (b) Hong, X.; Trost, B. M.; Houk, K. N. *J. Am. Chem. Soc.* **2013**, *135*, 6588. (c) Dang, Y.; Qu, S.; Wang, Z.-X.; Wang, X. *J. Am. Chem. Soc.* **2014**, *136*, 986.
(23) (a) Trost, B. M.; Imi, K.; Indolese, A. F. *J. Am. Chem. Soc.* **1993**, *115*, 8831. (b) Varela, J. A.; Rubín, S. G.; González-Rodríguez, C.; Castedo, L.; Saá, C. *J. Am. Chem. Soc.* **2006**, *128*, 9262. (c) García-Rubín, S.; Varela, J. A.; Castedo, L.; Saá, C. *Chem.—Eur. J.* **2008**, *14*, 9772.
(24) Schneebeli, S. T.; Hall, M. L.; Breslow, R.; Friesner, R. *J. Am. Chem. Soc.* **2009**, *131*, 3965.
(25) (a) Le Paih, J.; Dérien, S.; Dixneuf, P. H. *Chem. Commun.* **1999**, 1437. (b) Le Paih, J.; Monnier, F.; Dérien, S.; Dixneuf, P. H.; Clot, E.; Eisenstein, O. *J. Am. Chem. Soc.* **2003**, *125*, 11964. (c) Yamamoto, Y. *Organometallics* **2013**, *32*, 5201.
(26) (a) Ernst, C.; Walter, O.; Dinjus, E.; Arzberger, S.; Gorls, H. *J. Prakt. Chem.* **1999**, *341*, 801. (b) Ernst, C.; Walter, O.; Dinjus, E. *J. Organomet. Chem.* **2001**, *627*, 249. (c) Yamamoto, Y.; Arakawa, T.; Itoh, K. *Organometallics* **2004**, *23*, 3610. (d) Yamamoto, Y.; Kataoka, H.; Kinpara, K.; Nishiyama, H.; Itoh, K. *Lett. Org. Chem.* **2005**, *2*, 219. (e) Zhang, L.; Sung, H. H.-Y.; Williams, I. D.; Lin, Z.; Jia, G. *Organometallics* **2008**, *27*, 5122. (f) Also see refs 3 and 24.
(27) For comparison purposes, **IM10** and **IM16** are drawn as their mirror images in Scheme 5.
(28) (a) Merlic, C. A.; Pauly, M. E. *J. Am. Chem. Soc.* **1996**, *118*, 11319. (b) Wang, Y.; Finn, M. G. *J. Am. Chem. Soc.* **1995**, *117*, 8045. (c) Maeyama, K.; Iwasawa, N. *J. Org. Chem.* **1999**, *64*, 1344. (d) Miura, T.; Iwasawa, N. *J. Am. Chem. Soc.* **2002**, *124*, 518. (e) O'Connor, J. M.; Friese, S. J.; Tichenor, M. *J. Am. Chem. Soc.* **2002**, *124*, 3506. (f) Martin-Matute, B.; Nevado, C.; Cardenas, D. J.; Echavarren, A. M. *J. Am. Chem. Soc.* **2003**, *125*, 5757.
(29) (a) Wakatsuki, Y. *J. Organomet. Chem.* **2004**, *689*, 4092. (b) Lynam, J. M. *Chem.—Eur. J.* **2010**, *16*, 8238. (c) Bruneau, C.; Dixneuf, P. H. *Angew. Chem., Int. Ed.* **2006**, *45*, 2176.
(30) (a) De Angelis, F.; Sgamellotti, A. *Organometallics* **2002**, *21*, 5944. (b) De Angelis, F.; Sgamellotti, A. *Organometallics* **2002**, *21*, 2715. (c) Wakatsuki, Y.; Koga, N.; Yamazaki, H.; Morokuma, K. *J. Am. Chem. Soc.* **1994**, *116*, 8105. (d) Tokunaga, M.; Suzuki, T.; Koga, N.; Fukushima, T.; Horiuchi, A.; Wakatsuki, Y. *J. Am. Chem. Soc.* **2001**, *123*, 11917. (e) Peréz-Carreño, E.; Paoli, P.; Ienco, A.; Mealli, C. *Eur. J. Inorg. Chem.* **1999**, 1315. (f) Wakatsuki, Y.; Koga, N.; Werner, H.; Morokuma, K. *J. Am. Chem. Soc.* **1997**, *119*, 360. (g) Cabeza, J. A.; Pérez-Carreño, E. *Organometallics* **2010**, *29*, 3973.
(31) (a) Grotjahn, D. B.; Zeng, X.; Cooksy, A. L. *J. Am. Chem. Soc.* **2006**, *128*, 2798. (b) Grotjahn, D. B.; Zeng, X.; Cooksy, A. L.; Kassel, W. S.; DiPasquale, A. G.; Zakharov, L. N.; Rheingold, A. L. *Organometallics* **2007**, *26*, 3385. (c) De Angelis, F.; Sgamellotti, A.; Re, N. *Organometallics* **2007**, *26*, 5285. (d) Vastine, B. A.; Hall, M. B. *Organometallics* **2008**, *27*, 4325. (e) Cowley, M. J.; Lynam, J. M.; Slattery, J. M. *Dalton Trans.* **2008**, 4552. (f) Dang, Y.; Qu, S.; Wang, Z.-X.; Wang, X. *Organometallics* **2013**, *32*, 2804.
(32) (a) Bly, R. S.; Silverman, G. S.; Bly, R. K. *J. Am. Chem. Soc.* **1988**, *110*, 7730. (b) Roger, C.; Bodner, G. S.; Hatton, W. G.; Gladysz, J. A. *Organometallics* **1991**, *10*, 3266. (c) Kusama, H.; Takaya, J.; Iwasawa, N. *J. Am. Chem. Soc.* **2002**, *124*, 11592.